Title

Avidity-based method for selective purification of monoubiquitinated recombinant proteins for biophysical analysis

Author

Nelson, Spencer Louis

Publication Date

2022

Peer reviewed|Thesis/dissertation

UNIVERSITY OF CALIFORNIA SAN DIEGO

Avidity-based method for selective purification of monoubiquitinated recombinant proteins for biophysical analysis

A Thesis submitted in partial satisfaction of the requirements
for the degree Master of Science

in

Chemistry

by

Spencer L. Nelson

Committee in charge:

Professor Lalit Deshmukh, Chair
Professor Gourisankar Ghosh
Professor Patricia A. Jennings

2022

The Thesis of Spencer L. Nelson is approved, and it is acceptable in quality and form for publication on microfilm and electronically.

University of California San Diego

2022

DEDICATION

This manuscript is dedicated to my father, Alan Nelson, who inspired me at a young age to study the physical world. The work here would not have been achieved without his continued support in all aspects of my life.

TABLE OF CONTENTS

LIST OF FIGURES

LIST OF TABLES

LIST OF ABBREVIATIONS

ALIX	apoptosis-linked gene-2-interacting protein X
NEDD4	Neuronal precursor cell-expressed developmentally downregulated 4
FRAP	fluorescence recovery after photobleaching
UbE1	ubiquitin-activating enzyme
UbE2D3	ubiquitin conjugating enzyme E2 D3
NEDD4L	NEDD4 like E3 ubiquitin protein ligase
WWP2	WW domain containing E3 ubiquitin protein ligase 2
ESCRT	endosomal sorting complex required for transport
GPCR	G protein coupled receptors
HIV-1	human immunodeficiency virus 1
TEV	tobacco etch virus
NMR	nuclear magnetic resonance
RDC	residual dipolar coupling
NHS	H-hydroxysuccinimide
SDS-PAGE	sodium dodecyl-sulfate polyacrylamide gel electrophoresis
LC-MS	liquid-chromatography-mass spectrometry
PEG	polyethylene glycol
EM	electron microscopy
SUMO	small ubiquitin-related modifier

ACKNOWLEDGEMENTS

First and foremost, I would like to acknowledge my mentor, Dr. Lalit Deshmukh, for taking me on as a student, teaching me practically everything I know now about proteins and pushing me to accomplish what I believe is a successful project. I would also like to acknowledge my colleagues and lab-mates Ruben D. Elias, Chenrong Yu, and Amon Shihora for keeping me motivated, offering useful insights, and assisting me with numerous tasks in thelab. A special thanks to Dr. Itay Budin and all members of the Budin lab for the use of equipment, sharing of supplies, and teaching me new techniques for GUV formation. I would also like to express my gratitude to Simone Hall of the McHugh lab for always responding to my emails and assisting me with their LI-COR instrument for the western blot images I used in this thesis. I would also like to recognize my thesis committee members, Dr. Patricia Jennings and Gourisankar Ghosh, for their continued support and guidance.

I would like to give special thanks to Dr. Guillaume Castillon for TEM assistance, Dr. Peng Guo for microscopy training and troubleshooting, Dr. Xuemei Huang for NMR assistance, and Dr. Yongxuan Su for excellent and timely LC-MS verification of all protein masses. Additionally, I would like to express my appreciation and gratitude to our collaborators, Dr. Yue Chen and Ms. Yunan Li, from the University of Minnesota, for graciously accepting to participate in our research project and providing invaluable data regarding the site specificity of our ubiquitinated proteins.

Lastly, I would like to express how grateful I am to my friends and family that I had throughout my master's program for keeping me sane, making me insane, and always supporting me no matter the case. Special thanks to my mother for her continual support, my father for keeping me housed, and to my best friend Aaron Navarro for ensuring I always had

a friend that could brighten my day. Lastly, I would like to thank my sister, Sierra Nelson, for moving down to San Diego, enjoying time with me, and always being concerned about my welfare. Without them, I surely would not have succeeded.

Chapter 1, in full, has been submitted for publication of the material as it may appear in the Journal of the American Chemical Society, 2022, Nelson Spencer; Li, Yunan; Chen, Yue; Deshmukh, Lalit. “Avidity-based method for the efficient generation of monoubiquitinated recombinant proteins”. The -author of the thesis was the primary researcher and author of this paper.

VITA

2018 Bachelor of Science in Chemistry, University of California San Diego

2018-2020 Scientist I, Eurofins Advantar

2022 Master of Science in Chemistry, University of California San Diego

PUBLICATIONS

Ramaraju B, **Nelson SL,** Zheng W, Ghirlando R, Deshmukh L. Quantitative NMR study of insulin degrading enzyme using amyloid-β and HIV-1 p6 elucidates its chaperone activity. Biochemistry. 2021;60(33):2519-2523. doi:10.1021/acs.biochem.1c00342

Nelson SL; Li, Y; Chen, Y; Deshmukh L. Avidity-based method for the efficient generation of monoubiquitinated recombinant proteins. Submitted

ABSTRACT OF THE THESIS

Avidity-based method for selective purification of monoubiquitinated recombinant proteins for biophysical analysis

by

Spencer Nelson

Master of Science in Chemistry

University of California San Diego, 2022

Professor Lalit Deshmukh, Chair

Protein ubiquitination is a highly conserved posttranslational modification in which the protein ubiquitin is covalently linked through an isopeptide bond to a lysine residue of the target protein. Proteins can be mono-, multimono-, or poly-ubiquitinated owing to ubiquitin's seven lysine residues and N-terminal methionine, which create unique topologies and codes that can be interpreted by cellular ubiquitin receptors. Among these modifications, monoubiquitination

is the most abundant and participates in a myriad of cellular processes, including protein degradation, trafficking, DNA repair, viral budding, and neurodegenerative proteinopathies. Here we demonstrate an avidity-based method that we developed, which can produce monoubiquitinated recombinant proteins with native isopeptide bonds in yields and purities sufficient for biophysical characterization. As a proof of concept, we used this method to monoubiquitinate two specific proteins, Parkinson's protein α-synuclein and ESCRT-protein ALIX, using native NEDD4-family E3 ligases. Using quantitative chemical proteomics, we identified ubiquitination hotspots for NEDD4L-mediated monoubiquitination of α-synuclein and NEDDL, as well as WWP2-mediated monoubiquitination of ALIX. Additionally, we uncovered strikingly opposite effects of monoubiquitination on the phase separation and fibrillization properties of these two amyloidogenic proteins, thereby providing unique insights into the impact of monoubiquitination on protein aggregation.

INTRODUCTION

Section 1: Ubiquitination

Ubiquitin is a highly conserved, 76-residue protein (Fig. 1A), which acts as a reversible post-translational modification that signals for numerous cellular processes, including protein degradation, DNA repair, viral budding, endocytosis, and protein trafficking[1-5]. Ubiquitination is controlled by a three-step enzymatic cascade consisting of ubiquitin activating enzyme E1, a ubiquitin conjugating enzyme E2, and a ubiquitin ligating enzyme E3 (Fig.1B). The E1 initiates the cascade via acyl-adenylation of the C-terminal glycine of ubiquitin, which is then attacked by the reactive cysteine, forming a high-energy thiol ester[6]. Once the ubiquitin is primed, the E1 can transfer the ubiquitin to the active cysteine of an E2. The E3 then recruits both the E2 and the substrate, enabling the E2 to catalyze the formation of an isopeptide linkage between the C-terminus of ubiquitin and the substrate's lysine. Note that for HECT (homologous to the E6-AP carboxyl terminus) domain containing E3 ligases, such as those in the NEDD4 (neural precursor cell expressed developmentally down-regulated protein 4) family, the E2 will transfer the ubiquitin first to the HECT domain's active cysteine and the E3 will then directly ligate ubiquitin onto the substrate. This contrasts with the vast majority of E3 ligases that contain RING (really interesting new gene) domains, such as members of the U-box family, where the E3 contains Zn^{2+} coordinated through cysteine and histidine residues that aid in the transfer of ubiquitin from the E2 to the substrate. RING domains do not contain catalytically active cysteines that form thiol ester bonds with ubiquitin as the HECT domain do[7].

Ubiquitin comprises seven native lysine residues and one methionine (Fig. 1A), each of which can be ubiquitinated, culminating in topographically unique polyubiquitin chains[8]. Thus, target proteins can be decorated with ubiquitin in various ways A protein can be monoubiquitinated

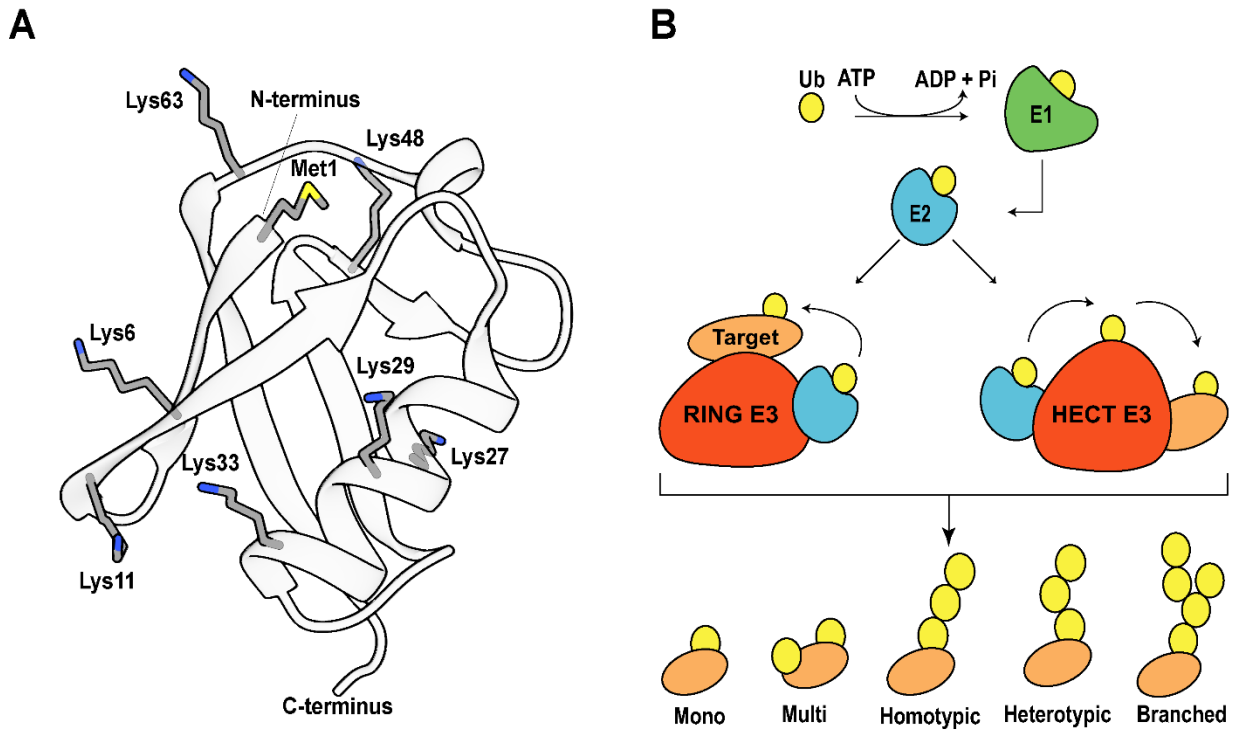

Figure 1 Ubiquitin and the ubiquitin enzymatic cascade

(**A**) Ubiquitin (PDB entry: 1UBQ)[9] with its seven native lysine and one methionine depicted in ball and stick representation . (**B**) Schematic of the ubiquitin enzymatic cascade with either a RING domain containing E3 ligase or a HECT domain containing E3. Note that RING E3s do not contain a catalytically active cysteine and the E2 transfers ubiquitin directly onto the substrate's target lysine. HECT domain containing E3 ligases contain a catalytically active cysteine and the E2 transfers ubiquitin to the E3 which then attaches ubiquitin to the substrate's target lysine. The resulting ubiquitination products that can be generated are listed below

with a single ubiquitin attached to one lysine residue on the protein, or multi-mono-ubiquitinated with multiple -ubiquitin moieties conjugated to different lysine residues of the target protein. Alternatively, a protein can be polyubiquitinated, where a ubiquitin chain is conjugated to the protein. The chain can be homotypic, where each ubiquitin moiety is linked through the same ubiquitin lysine, or heterotypic, with different linkages being present within the chain. Furthermore, branched polyubiquitin chains can form, adding additional complexity to the chain structure.

The ability of ubiquitin to form topologically distinct structures on a target protein aids in its ability to control cellular signaling. The plethora of signals that ubiquitin structures encode are often referred to as the "ubiquitin code"[10]. To interpret these ubiquitin codes, cells contain a variety of UBDs (ubiquitin-binding domains), which can bind and discriminate between the different ubiquitin topologies. UBDs are structurally diverse and include α-helical structures like UBA (ubiquitin associated domain), UIM (ubiquitin interacting motif), inverted UIMs, - and UEV (ubiquitin E2 variant), as well as zinc fingers, and PH (plekstrin homology) folds, among others[11-12]. UBDs recognize ubiquitin chain topologies by unique multivalent interactions between ubiquitin chains and the UBD. Additionally, DUBs (deubiquitinating enzymes) recognize ubiquitin chains, and ensure recycling of ubiquitin[13]. While polyubiquitin codes have been well studied, much less is known about the signals and processes controlled by monoubiquitination. How monoubiquitin regulates cell signaling and how its dysregulation leads to pathologies are of growing interest in the field of ubiquitination.

Section 2: Monoubiquitination

Monoubiquitination is the most abundant form of cellular ubiquitination[14]. However, it has been relatively unexplored compared to polyubiquitinated proteins. Monoubiquitination is importance for numerous cellular functions including transcription regulation, DNA repair, endocytosis and degradation, and signal transduction[15]. This is because monoubiquitination enables additional interaction interfaces, and through these changes it modifies the underlying protein-protein interactions. Below are listed some of the known cellular roles of monoubiquitination:

1) Transcription regulation: Monoubiquitination of lysine 119 of histone H2A is associated with gene silencing by promoting recruitment of Polycomb group proteins

from Polycomb repressor complex 1 resulting in suppression of transcription at this location[16]. Interestingly, this has an opposite effect on transcription when histone H2B is monoubiquitinated, as this promotes recruitment of transcription factors and aids in remodeling of the chromatin structure to enable easier access to protein complexes necessary for transcription[17]. Additional transcriptional control is mediated by monoubiquitination of transcriptional factors which can promote activity through enhanced protein-protein interactions as is the case with CIITA (class II transactivator) and MHC-II (major histocompatibility complex II)[18]. Alternatively, monoubiquitination of ΔNp63α regulates its transcriptional repressor activity by interfering with ΔNp63α-DNA binding interactions[19].

2) Endo-lysosomal pathway: Membrane proteins such as receptor tyrosine kinases and GPCRs (G-protein coupled receptors) rely on ubiquitination for their internalization and proper trafficking to endosomes. When these proteins are monoubiquitinated, they recruit the appropriate complexes for sorting via the trans-Golgi network, where they are sorted to endocytic compartments and directed to the lysosome for degradation[20].
3) Proteasomal degradation: Monoubiquitination is also sufficient for targeted degradation of proteins by the proteasome, where it is recognized by the proteasome's ubiquitin receptors Rpn10 and Rpn13, although this is generally limited to smaller proteins (<150 residues)[1]. Interestingly, these ubiquitin receptors are themselves modified by monoubiquitin, which regulates substrate recruitment to the proteasome[21].

Dysregulation of monoubiquitination is associated with numerous pathologies. For example, it is implicated in the development of PD (Parkinson's Disease). PD results from the death of dopaminergic neurons in the substantia nigra with the development of α-synuclein rich

inclusions, termed Lewey bodies, representing a hallmark of the disease. The E3 ligase SIAH (seven in absentia homolog) has been shown to monoubiquitinate α-synuclein resulting in the formation of cytotoxic α-synuclein aggregates[22]. Additionally, dysregulation of monoubiquitination of mitochondrial VDAC1 (voltage-dependent anion channel 1) could also contribute to PD[23]. Monoubiquitination of VDAC1 suppresses mitochondrial calcium uptake and without monoubiquitination, mitochondrial calcium uptake becomes dysregulated and apoptotic processes are induced[23]. Huntington's disease is another disease related to dysregulation of monoubiquitination. It is caused by abnormally long polyglutamine stretches within the huntingtin protein, which cause progressive deterioration of neuronal cells. Transcriptional dysregulation is a pathogenic mechanism of Huntington's disease, and disruption of monoubiquitination of histones has been implicated as the root cause[24]. Fanconi Anemia is a rare disease caused by a mutation in one of the 22 FANC (Fanconi anemia complementation) genes. The Fanconi anemia pathway has an important role in removal of DNA crosslinks and other chromosomal lesions. A key step in this repair pathway involves monoubiquitination of the FANCD2-FANCI complex to ensure conformational closure around the DNA[25]. However, in the disease state, successful monoubiquitination is abrogated and the repair pathway is heavily impaired[26].

Section 3: Approaches for Producing Ubiquitinated Proteins

Given the vast cellular and pathological processes governed by ubiquitination, it is important to understand how ubiquitination regulates these processes, how the conjugation of ubiquitin to target proteins alters their biophysical characteristics, and how dysregulation of protein ubiquitination results in pathology. Current methods for the production of ubiquitinated proteins can be categorized into two approaches[27]: enzymatic and semi-synthetic (chemical).

Enzymatic approaches utilize the native E1, E2 and E3 enzymes to ubiquitinate a target protein. While this can be easily achieved in vitro using recombinant enzymes and substrate, the resulting product is often a complex mixture of mono-, multi-mono-, and poly-ubiquitinated moieties. As monoubiquitination is the most prevalent form of cellular ubiquitination[14], it is a desirable product to obtain. However, the above-described in vitro enzymatic methods are typically unsuitable to produce purely monoubiquitinated protein. This is because selectively purifying monoubiquitinated species from the reaction mixture comprising mono- and poly-ubiquitinated species is technically difficult. Moreover, these methods generate heterogenous populations of mono-ubiquitinated substrate and are unsuitable for any controlled, site-specific modifications.

In some instances, site-specific modifications are desirable, such as when comparing aggregation kinetics of a substrate ubiquitinated at different sites or observing conformational changes in UBD containing proteins when ubiquitin is in different positions relative to the UBD. To achieve this, semisynthetic or chemical methods have been developed that allow site-specific ubiquitination and precise control of the subsequent chain length. Numerous chemical methods have been developed that employ disulfide linkages, thiol-ene chemistry, or even the use of synthetic amino acids to allow chemical conjugation of ubiquitin to a protein[28]. While powerful tools, these chemical approaches contain multiple difficulties that limit their widespread use, including technical complexity, loss of isopeptide similarity, low yields, and the constrained use of protein targets (i.e., only compatible with small proteins, proteins lacking a native cysteine, or the ones that are amenable to chemically harsh conditions)[28]. Therefore, there is a need for a more universal method that is compatible with a larger range of proteins, but still maintains simplicity and native isopeptide linkages. Owing to the ease of enzymatic ubiquitination reactions, it would

therefore be desirable to have a purification scheme that is capable of selectively purifying monoubiquitinated proteins from the complex reaction mixture. In Chapter 1, we demonstrate such a method that we developed, and utilize this approach to generate monoubiquitinated proteins of the Parkinson's protein α-synuclein and ESCRT-protein ALIX in yields and purity sufficient to analyze ubiquitin's impact on their biophysical characteristics.

Section 4: α-synuclein

α-synuclein (Fig. 2) is an amyloidogenic protein whose aggregation results in numerous pathological conditions, termed synucleinopathies, including Parkinson's disease (PD), dementia with Lewy bodies, and MSA (multiple system atrophy)[29]. These proteinopathies are represented by a loss of proteostasis resulting in accumulation of amyloidogenic aggregates of α-synuclein, and neuronal cell death. Various familial PD mutants of α-synuclein, including A30P, E46K, and A53T are observed to increase onset of the disease, and display increased aggregation kinetics[30]. α-synuclein is often degraded via the UPS (ubiquitin-proteasome system) and mono-ubiquitination of α-synuclein is sufficient for targeted degradation by the proteasome[31-32]. While the UPS degrades α-synuclein, α-synuclein is also capable of impairing the UPS[33]. Interactions between PD associated mutants, and the proteasome can inhibit the proteasome by occluding entrance into the complex thus preventing degradation of other substrates[34-35]. α-synuclein can also be degraded through chaperone mediated autophagy where is it recognized by hsp70 (heat shock protein of 70 kDa) chaperone and translocated through the lysosome via membrane receptor protein LAMP-2A (lysosome-associated membrane protein 2A). However, this pathway can be impaired due to PD mutants A30P and A53T, as they bind too tightly to LAMP-2A and are thus unable to translocate, blocking their degradation as well as the degradation of other proteins[36]. Alternatively, NEDD4 mediated K63 polyubiquitination of α-synuclein was shown to induce degradation through the

endosomal-lysosomal pathway[37]. As the disease state progresses and insoluble aggregates of α-synuclein begin to form, the autophagic pathway begins to degrade α-synuclein as well[38].

α-synuclein undergoes multiple post-translational modifications (Fig. 2). It is ubiquitinated and sumoylated at multiple lysine residues[39-40]. The ubiquitination and sumoylation of α-synuclein are used to target the protein for degradation through either the proteasome or lysosomal pathways, however, it also alters the aggregation tendencies of α-synuclein and may increase cytotoxicity of its aggregates[40]. Additionally, α-synuclein is phosphorylated at S87 and S129, with the latter defined as a hallmark of PD, and at residues Y125, Y133, and Y136, whose impact on synucleinopathies is not well understood [41-42]. The tyrosine residues of α-synuclein, namely Y39, Y125, Y133, and Y136, can also be nitrated, and are found to be important in α-synuclein aggregation[43-44]. Multiple threonine residues in α-synuclein have been found to be glycosylated which increases the toxicity of the by α-synuclein interfering with its membrane binding ability resulting in enhanced aggregation[45-46].

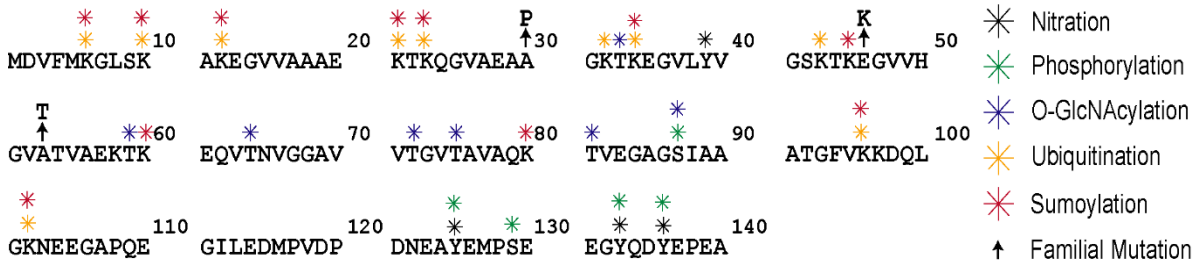

Figure 2 Familial mutations and post translational modifications of α-synuclein

Primary sequence of α-synuclein indicating locations of familial mutations (black arrow) and known post translation modifications including nitration (black), phosphorylation (green), O-GlcNAcylation (purple), ubiquitination (orange) and sumoylation (red).

α-synuclein aggregates found in Lewy bodies contain predominately mono- and di-ubiquitinated species[47]. Several E3 ligases have been identified that ubiquitinate α-synuclein in vivo including SIAH, Parkin, NEDD4, and NEDD4L[37, 48-49]. Additionally, NEDD4 family

proteins, namely NEDD4, NEDD4L, SMURF2 and ITCH, have been shown to ubiquitinate filamentous α-synuclein in vitro[50]. Ubiquitination of α-synuclein by NEDD4 proteins promotes degradation and clearance of α-synuclein, and by reducing α-synuclein content in cells, this may help prevent pathogenesis of α-synucleinopathies such as PD. NEDD4-mediated degradation of α-synuclein was demonstrated to protect against α-synuclein toxicity in Drosphilia and rodent models as well[51].

The impact of mono- and poly- ubiquitination on α-synuclein aggregation has previously been explored using semi-synthetic techniques to generate site specific ubiquitinated α-synuclein[52-53]. Monoubiquitination at residues K10 and K23 demonstrated similar levels of fibril formation when compared to unmodified α-synuclein, while K6, K12, and K21 showed some inhibition and ubiquitination at sites K32, K34, K43 and K96 showed strong inhibition of fibril formation[52]. Tetraubiquitination at residue K12 (with K48 linkages) of α-synuclein demonstrated chain length impact on aggregation with tetraubiquitinated α-synuclein forming nonamyloidogenic soluble aggregates as opposed to the fibrils associated with wild type α-synuclein[53]. These studies demonstrate ubiquitin's impact on the aggregation tendencies of α-synuclein, but do not explore its impact on liquid-liquid phase separation, nor take into consideration the heterogenous ubiquitin population that would exist in vivo and how that would impact the bulk aggregation tendencies.

Section 5: ALIX

ALIX (apoptosis-linked gene 2-interacting protein X) is an abundant cytosolic protein that functions within the ESCRT (endosomal-sorting complexes required for transport) pathway (Fig. 3). The ESCRT pathway comprises a collection of proteins that form polymeric filaments and mediate membrane scission to facilitate cytokinetic abscission, biogenesis of multivesicular bodies, plasma membrane repair, and budding of enveloped viruses such as HIV-1 and Ebola[54-56].

ALIX, also known as PDCD6IP (programmed cell death 6 interacting protein), is composed of a boomerang-shaped Bro1 domain, a coiled-coil V domain, and an unstructured C-terminal PRD (proline-rich domain; Fig. 3). The Bro1 domain of ALIX binds to and recruits the CHMP4 proteins, which are the main drivers of ESCRT-mediated membrane remodeling[55]. The ALIX V-domain binds to ubiquitin and K63-based polyubiquitin chains as well as the YPX(3)L motifs found in viral and cellular proteins[12, 57-58]. The PRD of ALIX contains multiple binding sites for an array of proteins. Our lab recently discovered that recombinant ALIX-PRD forms amyloid fibrils[59]. More intriguing is the reversible nature of these fibrils, as they dissolve upon hyperphosphorylation of ALIX-PRD mediated by Src kinase, and dephosphorylation by PTP1B (protein tyrosine phosphatase 1B) results in reformation of the fibrils[60]. Note that Src-mediated phosphorylation of ALIX regulates its cellular and membrane functions, while PTP1B has been shown to target the ESCRT machinery. Additionally, our lab recently showed that full-length ALIX undergoes phase separation in vitro and in vivo, mediated by its PRD, and that ALIX's phase separation plays a vital role in cytokinetic abscission, the last step of cell division.

ALIX, like many ESCRT-proteins, is monoubiquitinated in vivo. Monoubiquitination of ALIX is implicated in multiple processes, including endosomal protein sorting and retroviral budding (Fig. 3). The NEDD4 family ligase WWP2 is presumed to be responsible for ALIX monoubiquitination in the context of lysosomal degradation of GPCR PAR-1, and depletion of WWP2 inhibited ALIX ubiquitination and blocked successful sorting of this protein[61]. ALIX is also monoubiquitinated by NEDD4 and NEDD4L E3 ligases, implicated in HIV-1 budding[27, 62]. While it is evident that ubiquitination of ALIX is important, the exact mechanisms by which ubiquitin alters ALIX's function and biophysical characteristics remain elusive. Additionally, the

exact site of ALIX ubiquitination for these E3 ligases is unclear, and it is unknown whether different sites may have differential effects.

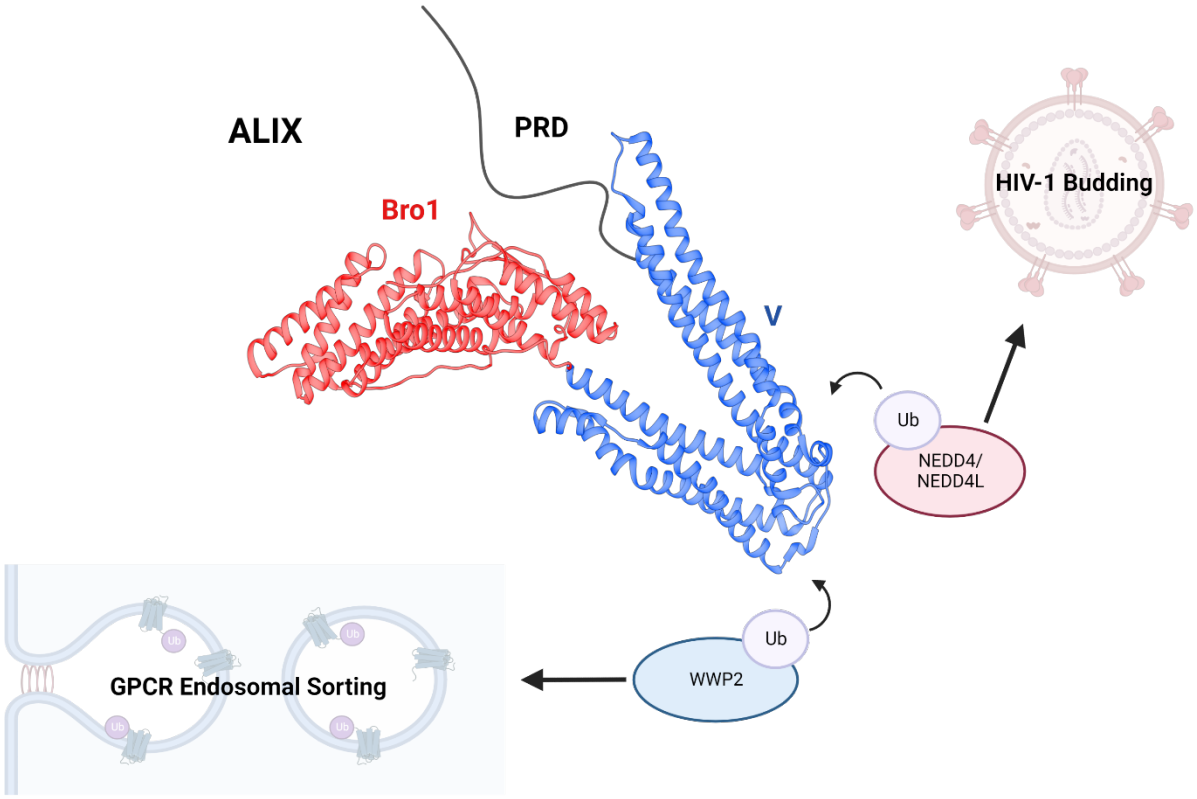

Figure 3 Membrane remodeling processes involving monoubiquitinated ALIX

Model of ALIX, based on X-ray structures of Bro1-V domains (PDB entry: 2XS1)[63]. Note that the structure of ALIX-PRD is not known as it is disordered. Monoubiquitination of ALIX mediates multiple membrane remodeling processes. ALIX monoubiquitination by E3 ligases NEDD4 and NEDD4L is implicated for HIV-1 budding while another NEDD4 family ligase WWP2 is necessary for successful endosomal sorting of GPCR[61-62].

CHAPTER 1

Avidity-based method for the efficient generation of monoubiquitinated recombinant proteins

Protein ubiquitination orchestrates nearly all eukaryotic cellular events.[64] It starts by attaching ubiquitin through isopeptide bonds to a single or multiple lysine residues of a target protein via a coordinated enzymatic reaction involving activating (E1), conjugating (E2), and ligating (E3) enzymes to form mono- or multi-mono-ubiquitinated products. Further modification of ubiquitin's seven lysine residues and its N-terminal methionine creates moieties decorated with polyubiquitin chains. These posttranslational modifications (mono-, multi-mono-, and poly-ubiquitination) encode specific signals that are decoded by deubiquitinating enzymes and proteins containing ubiquitin-binding domains. Among these, monoubiquitination is the most prevalent,[65] and is involved in various physiological processes (e.g., chromatin regulation, DNA damage response, protein sorting, trafficking, and degradation), viral egress, genetic disorders, and neurodegenerative proteinopathies.[15] Although the mechanisms that restrict the substrates to monoubiquitination, preventing polyubiquitination, are not clearly understood, monoubiquitinated proteins are often modified at multiple individual sites, creating a pool of heterogeneous populations.[22, 66] The frequency with which each site gets ubiquitinated and the collective effects of these modifications on the physicochemical characteristics of the target protein are usually unclear since obtaining such samples in sufficiently high yields and purities for biophysical studies is challenging. This is because enzymatic reactions performed on recombinant substrates often generate a composite mixture containing reaction components and mono-, multi-mono-, and poly-ubiquitinated products, and selective purification of monoubiquitinated species from this soup is difficult. Additionally, chemical (non-enzymatic) methods that can produce isopeptide-linked

monoubiquitinated proteins are technically challenging and not applicable to most proteins.[28] There is, therefore, a need for a technique that can facilitate the high-yield production of monoubiquitinated proteins. Here we present an efficient approach that fills this gap.

This method can be applied to recombinant substrates with specific ubiquitinating enzymes. As a proof-of-concept, we used two substrates, α-synuclein and ALIX, and enzymes UbE1, UbE2D3, and NEDD4-family E3 ligases (NEDD4L and WWP2); Fig. 4A. Aberrant aggregation of α-synuclein is a hallmark of Parkinson's disease.[67-68] α-synuclein accumulated in the Lewy bodies of Parkinson's patients is often mono- and di-ubiquitinated,[69] perhaps due to the breakdown of its cerebral degradation pathways. ESCRT-protein ALIX governs multiple processes, including endosomal protein sorting, neurodevelopment, cytokinesis, and enveloped virus budding.[59, 70-71] Like many ESCRT-proteins, ALIX undergoes monoubiquitination in vivo.[62, 72] All nine members of the NEDD4-family ligases collaborate with UbE1 and UbE2D3 to promote the ubiquitination of cellular proteins.[68] Specifically, NEDD4L ubiquitinates α-synuclein in the post-ischemic brain, promoting its degradation via the endolysosomal pathway,[73] whereas NEDD4L and WWP2 are involved in ALIX's monoubiquitination, vital for its roles in HIV-1 budding[27] and lysosomal sorting of GPCRs.[74] Although mono- and poly-ubiquitinated α-synuclein was produced using chemical methods,[75-77] no such attempts were made for ALIX, due to the problems associated with its recombinant expression stemming from ribosomal stalling induced by its amyloidogenic proline-rich domain (PRD).[59-60] We recently overcame these expression issues by introducing a P801G mutation in its PRD and established that ALIX phase separates via its PRD, crucial for its role in cytokinetic abscission.[78] However,

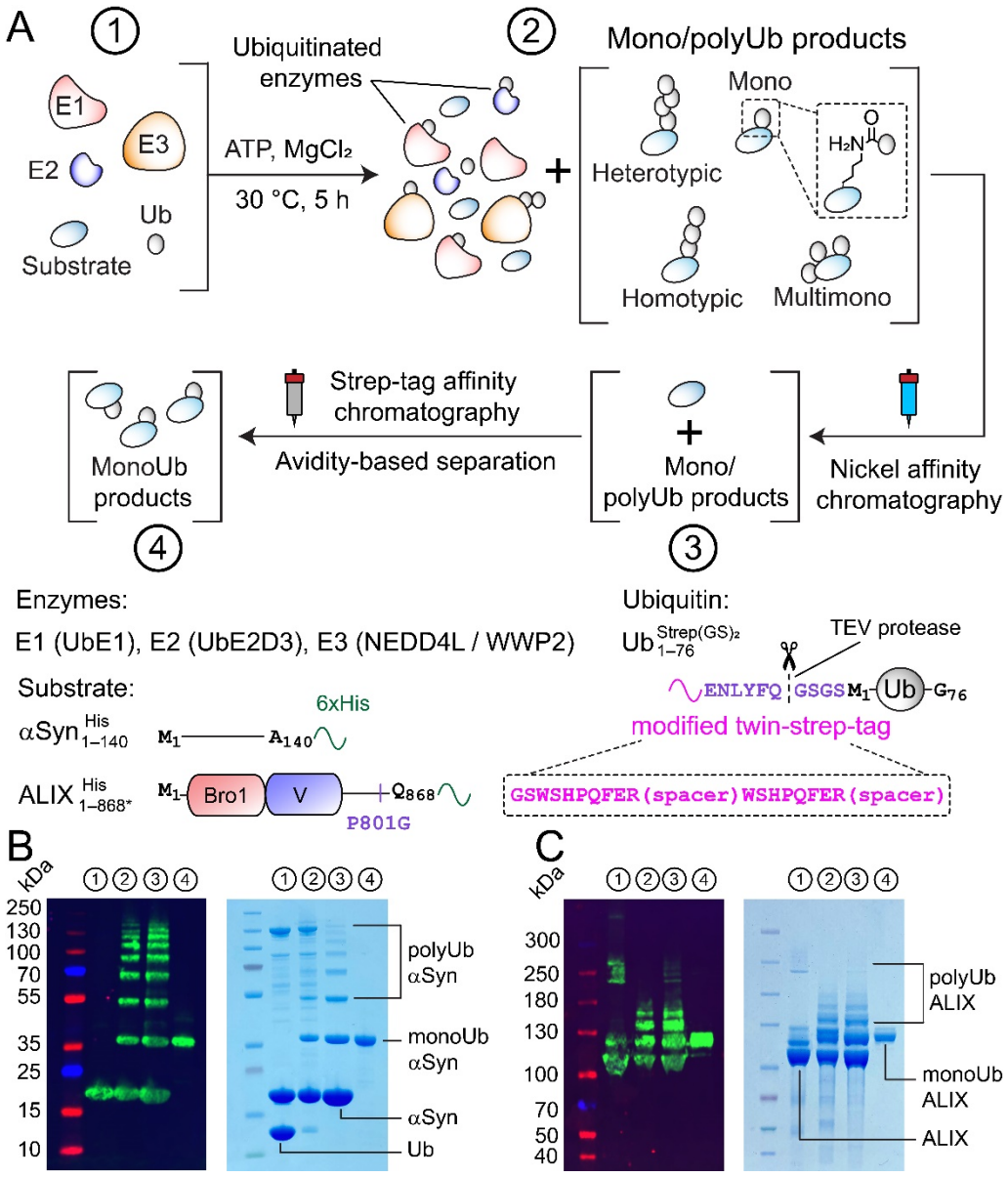

Figure 4 Large-scale production of monoubiquitinated proteins.

(**A**) In-vitro ubiquitination reaction where substrate, enzymes, and ubiquitin were mixed (Step 1), followed by the addition of ATP and $MgCl_2$ to produce mono-, multi-mono-, and poly-ubiquitinated products with native isopeptide linkages, highlighted in the dashed square (Step 2). The lower panel denotes the constructs that were used (Fig. 7 and Table 1). The reaction components were subjected to affinity chromatography (Steps 3 and 4) for a selective purification of monoubiquitinated products. Western blot and SDS-PAGE analyses of corresponding reactions of (**B**) $\alpha Syn^{His}_{1–140}$ + NEDD4L and (**C**) $ALIX^{His}_{1–868*}$ + WWP2; 4–12% Bis-Tris and 3–8% Tris-Acetate gels were used for $\alpha Syn^{His}_{1–140}$ and $ALIX^{His}_{1–868*}$, respectively. Aliquots from each step are designated by a circled number.

the effects of monoubiquitination on ALIX's aggregation are unclear, and how monoubiquitination affects its function remains unknown.

All recombinant enzymes were expressed with N-terminal polyhistidine affinity tags, which were cleaved using TEV-protease during the final stages of purification (SI Methods). α-synuclein and ALIX were expressed with non-cleavable C-terminal polyhistidine tags, $\alpha Syn^{His}_{1–140}$ and $ALIX^{His}_{1–868*}$ (the asterisk denotes P801G mutation), respectively; Fig. 4A. The ubiquitin construct carried a modified N-terminal twin-strep tag[79] and a TEV-protease cleavage site, $Ub^{Strep(GS)_2}_{1–76}$; see Fig. 7 for the rationale used for the design of this tag and Figs. 8-9 for the NMR chemical shift and RDC analyses of $Ub^{Strep(GS)_2}_{1–76}$, which revealed a minimal impact of the tag on ubiquitin's structure. The enzymes and $Ub^{Strep(GS)_2}_{1–76}$ were mixed with substrates ($\alpha Syn^{His}_{1–140}$/$ALIX^{His}_{1–868*}$) and incubated with ATP and $MgCl_2$ to generate mono-, multi-mono-, and poly-ubiquitinated products. Nickel affinity chromatography facilitated a selective purification of substrate and its ubiquitinated products. Monoubiquitinated species were separated from this mixture using strep-tag affinity chromatography by exploiting the avidity effect.[80] This is because unlike monoubiquitinated products, multi-mono-/poly-ubiquitinated moieties bound extremely tightly to the resin-coupled strep-tactin, a derivative of tetrameric streptavidin, and therefore, could not be readily displaced by the competitive binding reagent, biotin (Fig. 10). Western blot and SDS–PAGE analyses of $\alpha Syn^{His}_{1–140}$ + NEDD4L and $ALIX^{His}_{1–868*}$ + WWP2 reactions and purification of monoubiquitinated products are shown in Fig. 4B–C. Both reactions generated milligram quantities of monoubiquitinated products (Fig. 11 and Table 2), attesting to the efficacy of this method.

The high purity of the monoubiquitinated α-synuclein facilitated a detailed stoichiometric analysis using our chemical proteomics approach (Fig. 5A–C and SI Methods).[81] Here, unmodified

lysine residues of a target protein are conjugated to an acetyl-GG-NHS tag, followed by trypsin and glu-c digestion and secondary labeling with ^{13}C-acetyl-NHS, thereby generating fragments of the originally ubiquitinated peptides and their unmodified counterparts that are structurally identical but differ in ^{13}C-labeling (Fig. 5B). Subsequent LC–MS analysis of these fragments allows quantification of site-specific monoubiquitination frequency via a comparison of the corresponding chromatography peak-area ratios (Fig. 5C and Table 3). The N-terminal membrane binding region (MBR), central non-amyloid component (NAC), and C-terminal region (CTR) of α-synuclein were monoubiquitinated by NEDD4L at 37%, 21%, and 42%, respectively. The collective high-frequency (63%) of monoubiquitination of residues in the NAC (K80) and CTR (K96/K97/K102) of α-synuclein is consistent with the fact that NEDD4-ligases bind to the proline-rich region of its CTR.[68, 82] Although the stoichiometric deconvolution of immediately adjacent lysine residues (e.g., K96/K97/K102 of the CTR) was not feasible, we were able to quantify monoubiquitination frequencies for sufficiently distant residues of the MBR (e.g., 19% monoubiquitination at K6/K10/K12 vs. 10% at K21/K23). Similar stoichiometric quantification of cerebral α-synuclein is difficult owing to endogenous deubiquitinating enzymes and the rapid deubiquitination in postmortem samples.[82] Hence, the above approach identifies ubiquitination hotspots for a given group of enzymes and their substrate and provides important insights regarding the corresponding in vivo ubiquitination pattern for the said group.

Both unmodified and monoubiquitinated α-synuclein phase separated into spherical condensates with a molecular crowder PEG-8000, Figs. 5D and 12. Although freshly made condensates of both moieties were dynamic, as evidenced by FRAP assays (Fig. 5E), condensates of α-synuclein exhibited a noticeably lower fluorescence recovery than those of its

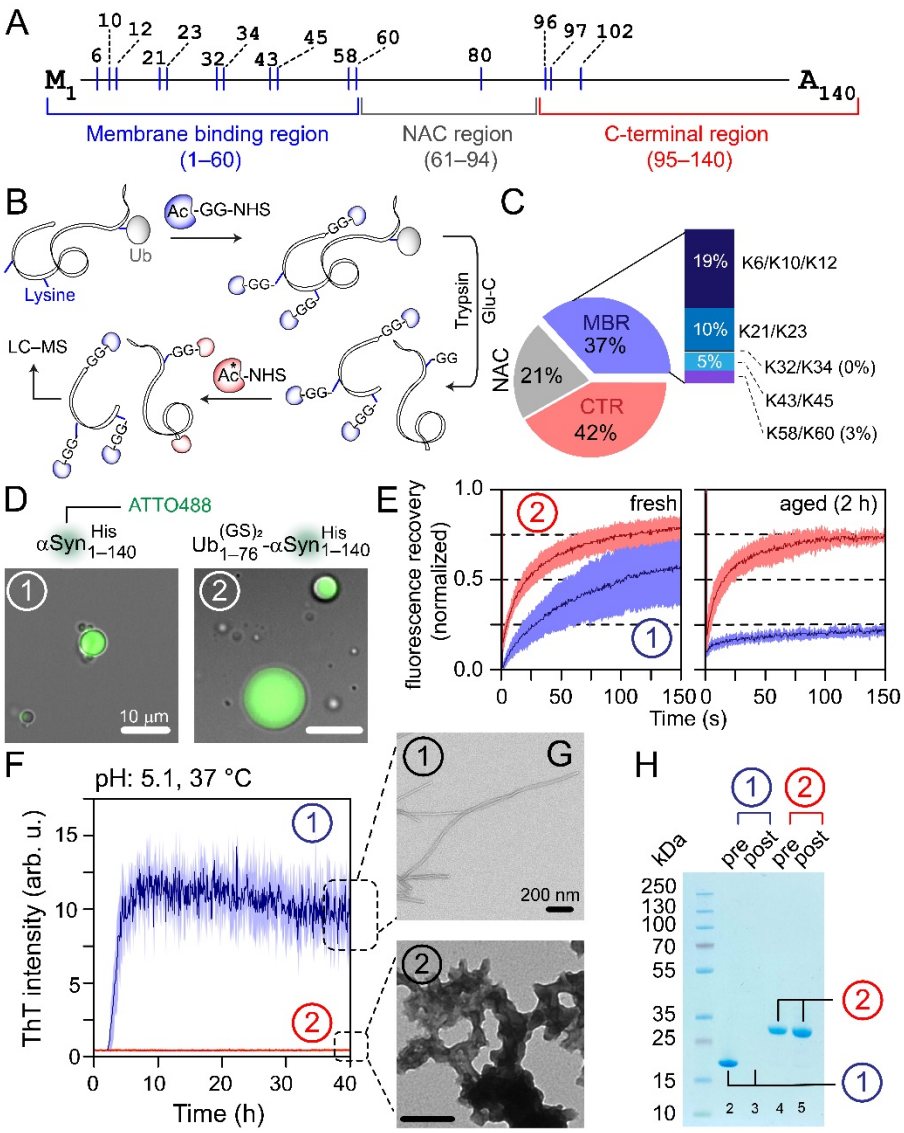

Figure 5 Impact of NEDD4L-mediated monoubiquitination on α-synuclein's aggregation.

(**A**) Scheme of α-synuclein, highlighting its regions and the location of its lysine residues. (**B**) Scheme of quantitative chemical proteomics used to determine monoubiquitination stoichiometry; the asterisk denotes ^{13}C-labeled acetyl-NHS. (**C**) Pie-chart of the average frequency of monoubiquitination in the MBR (blue), NAC (gray) and CTR (red) regions of $\alpha Syn^{His}_{1–140}$ (n = 2). Unlike the CTR, the monoubiquitination frequency for the individual lysine residues of MBR could be deconvoluted, represented by a stacked bar. (**D**) Microscopy images of droplets of ATTO488-labeled $\alpha Syn^{His}_{1–140}$ and its monoubiquitinated counterpart with 10% w/v PEG-8000, represented by circled no. 1 and 2, respectively; the same numbering scheme is used in the remaining panels. (**E**) FRAP analysis of freshly prepared and aged condensates with the solid line and shaded region representing the mean and SD (n = 3), and blue and red colors for unmodified and monoubiquitinated $\alpha Syn^{His}_{1–140}$, respectively. (**F**) Aggregation of non- and monoubiquitinated $\alpha Syn^{His}_{1–140}$ studied by ThT assays (n = 2); the same color-scheme as panel **E**. (**G**) Negative-stain EM images of aggregated samples from panel **F** showing ordered fibrils for $\alpha Syn^{His}_{1–140}$ and amorphous aggregates for its monoubiquitinated moieties. (**H**) SDS–PAGE analysis of pre- and post-aggregation of samples from panel **F**. The lack of band intensity in lane-3 is due to fibrillization of $\alpha Syn^{His}_{1–140}$.

monoubiquitinated counterpart (60% vs. 80% average recovery in 150 s, respectively). Moreover, the fluorescence recovery of α-synuclein condensates decreased significantly after a 2 h incubation at room temperature, whereas the condensates of monoubiquitinated α-synuclein remained dynamic (20% vs. 75% recovery, respectively). Additionally, the latter frequently coalesced and increased significantly in size with time. These observations indicate a time-dependent increase in the gelation of α-synuclein droplets, perhaps due to its fibrillization and the lack thereof for its monoubiquitinated moieties. Aggregation assays performed using an amyloid-sensitive dye, Thioflavin T (ThT), confirmed this hypothesis, with sigmoidal aggregation profiles for α-synuclein, a hallmark of fibrillization, and no obvious ThT signals for its monoubiquitinated counterpart (Fig. 5F). Negative-stain EM and SDS–PAGE and analyses demonstrated the presence of SDS- resistant fibrils and nonfibrillar aggregates for unmodified and monoubiquitinated α-synuclein, respectively (Fig. 5G–H). These results show that NEDD4L-mediated monoubiquitination of α-synuclein creates dynamic condensates and makes it resistant to fibrillization.

Solution NMR analysis established that the ALIX-V domain binds to ubiquitin, Figs. 6A–B and 13, consistent with a prior report that measured a dissociation constant of ~120 μM for this interaction.[83] Analysis of monoubiquitinated $ALIX^{His}_{1–868*}$ using quantitative chemical proteomics showed that the V-domain is significantly more monoubiquitinated by NEDD4L and WWP2 (74% and 60% monoubiquitination, respectively, Fig. 6C and Table 3) than Bro1 and PRD of ALIX. Examination of site-specific frequencies revealed two significant differences (Fig. 6D). Residues K501/K510 of V-domain were monoubiquitinated at 38% vs. 8% while residue K420 was monoubiquitinated at 13% vs. 26% by NEDD4L and WWP2, respectively, highlighting the site-specific preferences of these two NEDD4-family ligases. ALIX and its

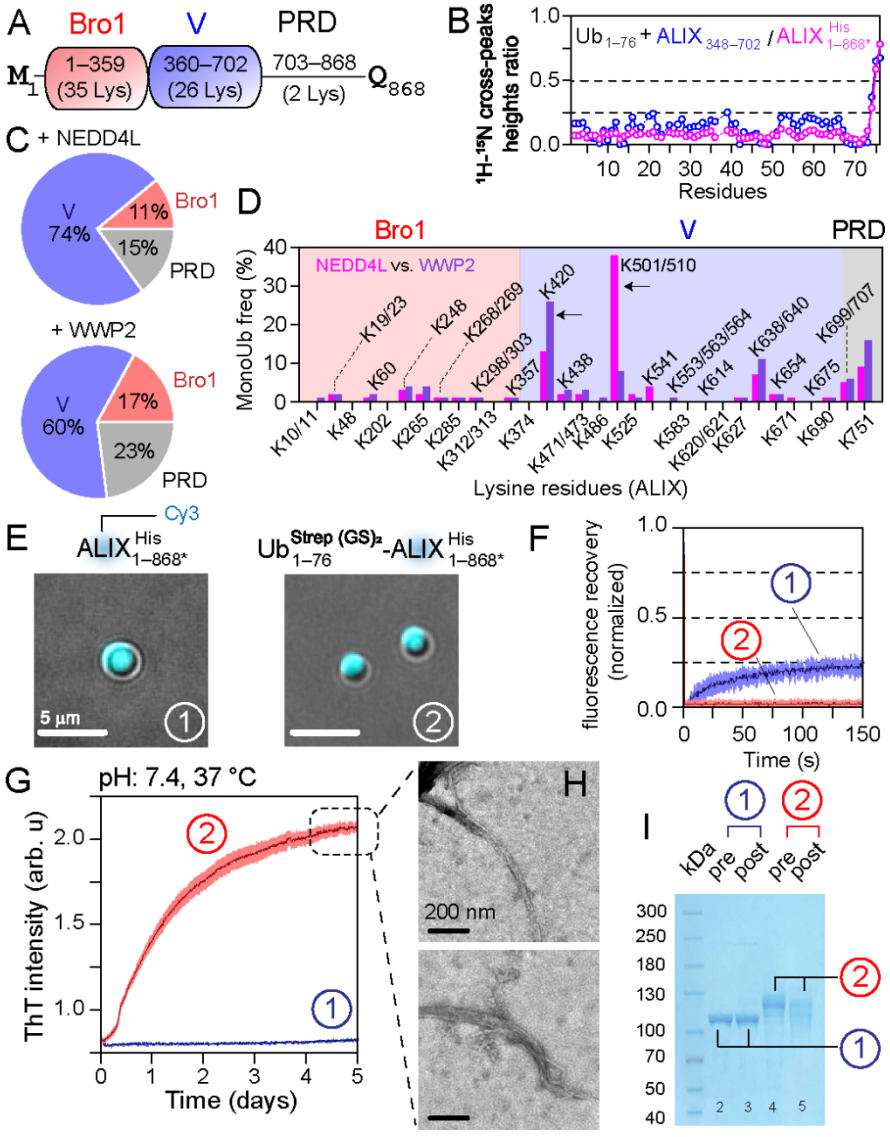

Figure 6 NEDD4L/WWP2-mediated monoubiquitination of ALIX.

(**A**) Scheme of ALIX, highlighting its domains and the number of lysine residues in each domain (Fig. 14). (**B**) The reduction in $^{1}H_{N}/^{15}N$ cross-peak heights of 100 µM ^{15}N-labeled ubiquitin with 100 µM non-labeled $ALIX_{348–702}$ (blue) and $ALIX^{His}_{1–868*}$ (pink). (**C**) Pie charts illustrating the average frequency of monoubiquitination in individual ALIX domains using NEDD4L (upper) and WWP2 (lower); n = 2. (**D**) Bar-chart of site-specific differences in monoubiquitination frequencies of ALIX residues brought out by NEDD4L (pink) and WWP2 (magenta); arrows mark significant differences. Only ubiquitinated residues are plotted. (**E**) Microscopy images of condensates of Cy3-labeled $ALIX^{His}_{1–868*}$ and its WWP2-mediated monoubiquitinated counterpart (5% w/v PEG-4000), represented by circled no. 1 and 2; the same numbering scheme is used in the remaining panels. (**F**) Poor FRAP recoveries (< 25%) for the freshly prepared condensates of $ALIX^{His}_{1–868*}$ (blue) and its WWP2-mediated monoubiquitinated moieties (red), n =3, the same coloring scheme in the remaining panels. (**G**) Fibrillization of monoubiquitinated $ALIX^{His}_{1–868*}$ and the lack thereof for its nonubiquitinated species by ThT assays, n = 2. (**H**) Negative-stain EM analyses of fibrils formed by monoubiquitinated $ALIX^{His}_{1–868*}$. (**I**) SDS–PAGE analysis of pre- and post-aggregation of samples from panel **G**. Fibrillization of monoubiquitinated ALIX resulted in a decreased band intensity in lane-5 as compared to the pre-aggregation sample in lane-4.

monoubiquitinated counterpart formed gel-like condensates with PEG-4000, as evidenced by fluorescence microscopy and negligible FRAP recoveries (Figs. 6E–F and 12), consistent with our recent findings that ALIX makes gel-like condensates that confine abscission factors.[78] Unlike α-synuclein (cf. Fig. 5E), monoubiquitinated ALIX did not form dynamic condensates, possibly because monoubiquitinated ALIX molecules bound to one another via their V-domains, thereby creating optimal conditions for nucleation and growth of ALIX fibrils. ThT assays, negative-stain EM, and SDS-PAGE analyses confirmed this hypothesis and revealed that, in contrast to unmodified ALIX, its monoubiquitinated counterpart formed amyloid fibrils (Fig. 6G–I). Such fibrils in vivo will likely act as a scaffolding platform, aiding the formation of downstream ESCRT filaments needed for membrane scission, thereby facilitating ALIX's versatile functions.

In summary, we devised an efficient method to produce monoubiquitinated proteins. We identified ubiquitination hotspots and uncovered the impact of monoubiquitination on the phase separation and fibrillization properties of α-synuclein and ALIX. Given its ease-of-use, this method will apply to many similar systems and lays a solid foundation for our ongoing efforts to produce specifically monoubiquitinated and polyubiquitinated recombinant proteins. Additionally, it will serve as a template to generate SUMOylated proteins,[84] a posttranslational modification analogous to ubiquitination.

SUPPLEMENTARY INFORMATION

Materials and methods.

Materials.

Polyethylene glycol-4000 (PEG-4000) and PEG-8000 were purchased from Sigma-Aldrich (catalog no. 81240 and 81268, respectively). Fluorescent dyes, ATTO-488 N-hydroxysuccinimide (NHS) ester and Cy3 maleimide, were purchased from ATTO-TEC GmbH (catalog no. AD 488-

31) and Cytiva (catalog no. PA13131), respectively. Both dyes were dissolved in dimethylformamide before use. Adenosine 5'-triphosphate (ATP) was purchased from Sigma-Aldrich (catalog no. A2383). α-synuclein and ALIX monoclonal primary antibodies for western blotting were purchased from Thermo Fisher Scientific (catalog no. AHB0261 and MA1-83977, respectively). The secondary antibody, IRDye 800CW, was purchased from LI-COR Biosciences (catalog no. 925-32210). Gels for sodium dodecyl sulfate polyacrylamide gel electrophoresis (SDS-PAGE) were purchased from Thermo Fisher Scientific (4–12% Bis-Tris and 3–8% Tris-Acetate gels, catalog no. NW04122BOX and EA0378BOX, respectively). Reagents for nuclear magnetic resonance (NMR) isotopic enrichment were obtained from Cambridge isotope laboratories and Sigma-Aldrich. Ingredients for NMR alignment medium, namely PEG monododecyl ether and 1-hexanol, were obtained from Sigma-Aldrich (catalog no. 76437 and H13303, respectively).

Methods.

Recombinant protein expression and purification.

Constructs used in current study, namely ubiquitinating enzymes, substrates, and modified twin-strep tagged ubiquitin, were custom synthesized from Azenta Life Sciences; see Fig. 4A for the design and Table 1 for subcloning of each construct. Constructs of tobacco etch virus (TEV) protease and wild-type ubiquitin, $Ub_{1–76}$, were generous gifts from David S. Waugh (NCI) and G. Marius Clore (NIDDK), respectively. TEV protease, $Ub_{1–76}$, and $\alpha Syn^{His}_{1–140}$ were expressed at 37 °C. All remaining constructs were expressed at 16 °C. Cells were grown at 37 °C in 1 L Luria-Bertani (LB; MP Biomedicals, catalog no. 3002-036) medium or Terrific Broth (TB; Thermo Fisher Scientific, catalog no. BP9728-500) at natural isotopic abundance or minimal M9 medium[59-60] for isotopic labeling. Cells were induced with 1 mM isopropyl β-d-1-

thiogalactopyranoside (IPTG) and 0.2% (w/v) arabinose at an absorbance of 0.8 at 600 nm; note that arabinose was used in the case of BL21-AI competent cells.

The purification scheme of TEV protease has been described previously.[85] The enzymes UbE1, UbE2D3, UbE3-NEDD4L, and UbE3-WWP2 were purified using a combination of affinity and size-exclusion chromatography (ÄKTA Pure and Start protein purification systems, Cytiva). Briefly, cells were resuspended in a lysis buffer containing 50 mM Tris, pH 8.0, and 250 mM NaCl. Cells were lysed using EmulsiFlex-C3 (Avestin), and cleared by centrifugation (48,380g, 30 min). The cell lysates were loaded onto HisTrap columns (Cytiva). The bound enzymes were washed with 10 column volumes of the lysis buffer, followed by 10 column volumes of 30 mM imidazole, and eluted in the same buffer containing 500 mM imidazole. The eluted enzymes were concentrated (Amicon ultra-15 centrifugal filter units, 10/30 kDa cutoff; EMD Millipore) and loaded onto HiLoad 26/600 Superdex 200 pg or HiLoad 26/600 Superdex 75 pg (Cytiva) pre-equilibrated with 50 mM Tris, pH 8.0, 150 mM NaCl, 1 mM ethylenediaminetetraacetic acid (EDTA), and 1 mM dithiothreitol (DTT). The eluted enzymes were mixed with recombinant TEV protease (molar ratio 50:1) to hydrolyze polyhistidine affinity tags (total incubation time: ~ 20 h at room temperature). The subsequent reaction mixtures were loaded onto HisTrap columns, and the relevant flow-through fractions of TEV-cleaved enzymes were pooled, concentrated, and loaded onto HiLoad 26/600 Superdex 200 pg/HiLoad 26/600 Superdex 75 pg columns pre-equilibrated with 50 mM Tris, pH 8.0, 150 mM NaCl, 1 mM DTT, and 1 mM EDTA. Relevant UbE1/UbE2D3 fractions were concentrated (~ 5 mg/mL) and kept at -20 °C, whereas UbE3-NEDD4L/WWP2 fractions were pooled and kept at 4 °C.

For $\alpha Syn^{His}_{1–140}$, cells were resuspended in a lysis buffer containing 50 mM Tris, pH 8.0. Cells were lysed and cleared by centrifugation. The cell lysate was loaded onto a HisTrap column. The bound

protein was washed with 10 column volumes of the lysis buffer and eluted in the same buffer containing 500 mM imidazole. The eluted protein was loaded onto a Mono Q 10/100 GL anion-exchange chromatography column (Cytiva) with a 0–1 M NaCl gradient in a buffer containing 50 mM Tris, pH 8.0, and 1 mM EDTA. The eluted protein was further purified using high-performance liquid chromatography (HPLC; Jupiter 10 μm C18 300 Å column, Phenomenex; catalog no. 00G-4055-N0) with a 25–70% acetonitrile gradient comprising 0.1% trifluoroacetic acid (TFA; Sigma-Aldrich). The eluted fractions of $\alpha Syn^{His}_{1–140}$ were freeze-dried (Labconco -84 °C benchtop freeze dryer) and stored at -80 °C.

Cells expressing $ALIX^{His}_{1–868*}$, resuspended in a lysis buffer containing 50 mM Tris, pH 8.0, and 250 mM NaCl, were lysed and cleared by centrifugation. The cell lysate was loaded onto a HisTrap column. The bound protein was washed with 10 column volumes of the lysis buffer, 10 column volumes of 30 mM imidazole, and eluted in the same buffer containing 500 mM imidazole. The eluted protein was concentrated (Amicon ultra-15 centrifugal filter units, 30-kDa cutoff) and loaded onto a HiLoad 26/600 Superdex 200 pg column pre-equilibrated with 50 mM Tris, pH 8.0, 150 mM NaCl, 1 mM DTT, and 1 mM EDTA. Relevant fractions of $ALIX^{His}_{1–868*}$ were concentrated (~20 mg/mL) and stored at -20 °C.

For $ALIX_{348-702}$, a similar protocol as to that of $ALIX^{His}_{1–868*}$ was used. Briefly, the protein was purified using a combination of nickel affinity and size-exclusion chromatography. The eluted protein from the sizing (HiLoad 26/600 Superdex 75 pg) column was mixed with TEV protease to hydrolyze the B1 domain of protein G (GB1)-polyhistidine fusion tag.[86] The subsequent reaction mixture was loaded onto a HisTrap column, and the flow-through fractions of TEV-cleaved protein were pooled, concentrated, and loaded onto a HiLoad 26/600 Superdex 75 pg column pre-

equilibrated with 50 mM Tris, pH 8.0, 250 mM NaCl, and 1 mM DTT. Relevant fractions were pooled and kept at 4 °C.

Cells of $Ub_{1–76}^{Strep(GS)_2}$, resuspended in a lysis buffer containing 50 mM Tris, pH 8.0, 150 mM NaCl, and 1 mM EDTA, were lysed and cleared by centrifugation. The cell lysate was loaded onto an XK 16/20 chromatography column (Cytiva) prepacked with Strep-Tactin XT Sepharose resin (Cytiva). The bound protein was washed with 10 column volumes of the lysis buffer and eluted in the same buffer containing 50 mM biotin. The eluted protein was further purified using reverse-phase HPLC (Jupiter 10 μm C18 300 Å column, Phenomenex) with a 25–49% acetonitrile gradient comprising 0.1% TFA. The eluted fractions of $Ub_{1–76}^{Strep(GS)_2}$ were freeze-dried and stored at -20 °C. To hydrolyze modified twin-strep tag, lyophilized $Ub_{1–76}^{Strep(GS)_2}$ was reconstituted in ~100 μL buffer comprising 6 M guanidinium hydrochloride and 50 mM Tris, pH 8.0. Protein was exchanged into a buffer containing 50 mM Tris pH 8.0 and 1 mM DTT and subsequently mixed with TEV protease. The hydrolyzed product was purified using a combination of affinity chromatography and reverse-phase HPLC. The eluted fractions of $Ub_{1–76}^{(GS)_2}$ were freeze-dried and stored at -80 °C.

For wild-type ubiquitin, $Ub_{1–76}$, the cell lysate comprising 50 mM Tris (pH 7.5) was cleared by centrifugation and subsequently mixed with perchloric acid. The resultant mixture (pH 4) was further cleared by centrifugation (48,380g, 10 min) and loaded on a HiLoad 16/10 SP Sepharose HP column (Cytiva) pre-equilibrated in a buffer containing 50 mM sodium acetate, pH 4.5. The bound protein was eluted in the same buffer comprising a 0–1 M NaCl gradient. Relevant fractions were pooled and further purified using reverse-phase HPLC (Jupiter 10 μm C18 300 Å column, Phenomenex) with a 5–75% acetonitrile gradient comprising 0.1% TFA. The eluted protein was collected, freeze-dried, and stored at -20 °C until use.

All protein constructs and monoubiquitinated $\alpha Syn^{His}_{1–140}$ and $ALIX^{His}_{1–868*}$ were verified by mass spectrometry (MS) using our previously described protocol.[59-60, 85]

In vitro ubiquitination and purification of monoubiquitinated products.

Ubiquitinating enzymes (UbE1, UbE2D3, and UbE3-NEDD4L/WWP2), $Ub^{Strep(GS)_2}_{1–76}$, and substrate ($\alpha Syn^{His}_{1–140}$ / $ALIX^{His}_{1–868*}$) were mixed in a reaction buffer comprising 50 mM Tris, pH 7.5, 1 mM DTT, and 1 mM $MgCl_2$, Table S2. The reaction mixture was dialyzed against the same buffer with the addition of 1.5 mM ATP (total incubation time: 5 h at 30 °C). The resultant reaction was cleared by centrifugation and loaded onto a HisTrap column pre-equilibrated with a buffer containing 50 mM Tris, pH 8.0, and 250 mM NaCl. The bound components (i.e., the substrate and its ubiquitinated products) were eluted with 500 mM imidazole. The eluted proteins were loaded onto a XK 16/20 chromatography column prepacked with Strep-Tactin XT Sepharose resin (Cytiva) pre-equilibrated with buffer containing 50 mM Tris, pH 8.0, 150 mM NaCl, and 1 mM EDTA. The bound protein was eluted in the same buffer comprising a 0–50 mM biotin gradient. Relevant monoubiquitinated protein fractions were pooled and stored at -20 °C. The reaction progress and the subsequent purification of monoubiquitinated moieties were assessed using western blotting using our published protocol.[59-60] Blots were visualized using the Odyssey XF imaging system (LI-COR Biosciences).

For monoubiquitinated $\alpha Syn^{His}_{1–140}$, the modified twin-strep tag of $Ub^{Strep(GS)_2}_{1–76}$ was hydrolyzed using TEV protease. The resultant mixture was purified using reverse-phase HPLC (Jupiter 10 μm C18 300 Å column, Phenomenex) with a 35–45% acetonitrile gradient comprising 0.1% TFA. The eluted monoubiquitinated protein, $Ub^{(GS)_2}_{1–76}$-$\alpha Syn^{His}_{1–140}$, was collected, freeze-dried, and stored at -20 °C. These samples were used to determine the impact of monoubiquitination on the aggregation properties of α-synuclein. A similar procedure was not carried out for

monoubiquitinated ALIX, $Ub_{1-76}^{Strep(GS)_2}$-$ALIX_{1-868*}^{His}$, since the tag represented a minimal portion of the protein (3.45 kDa for the tag vs. 109.6 kDa for the monoubiquitinated ALIX).

Quantitative chemical proteomics.

Quantitative chemical proteomics was performed as previously described.[81] Briefly, ~5 µg of monoubiquitinated αSyn_{1-140}^{His} and $ALIX_{1-868*}^{His}$ were resuspended in 10 µL of 9 M urea in phosphate buffered saline (PBS). A labeling solution (100 mg/mL in 50% acetonitrile + 50% water) comprising amine-reactive chemical tag, acetyl glycylglycine-NHS (Ac-GG-NHS), was added to the samples with 1 µL each time and vortexing for 45 min. The labeling was repeated for a total of three times while maintaining a pH of 8–8.5. The reaction was quenched with the addition of 5% hydroxylamine (pH 6.0, 1.5 M) for 15 min. Samples were diluted by 1x PBS for six folds and digested by trypsin (Promega Corporation) at 37 °C overnight, followed by a second digestion with endoproteinase Glu-C (Sigma-Aldrich) for overnight at an enzyme-to-substrate ratio of 1:10 (w/w). Digested peptides were desalted with home-made C18 StageTip and dried in a SpeedVac vacuum concentrator (Thermo Fisher Scientific). Peptides were resuspended in 10 µl of 9 M urea in PBS. A labeling solution comprising heavy acetyl($^{13}CD_3$-^{13}CO)-NHS (100 mg/mL in 100% acetonitrile) was added to the peptide samples for the second labeling with 1 µL each time and vortexing for 45 min. The labeling was repeated for a total of three times and quenched with 5% hydroxylamine (pH 6.0, 1.5 M) for 15 min. The peptides were then desalted with StageTip and subjected to liquid chromatography (LC)–MS analysis (see below).

Peptides were dissolved in HPLC buffer A (0.1% formic acid in water) and injected into Dionex Ultimate 3000 RSLCnano-UPLC system (Thermo Fisher Scientific). Peptides were separated with a gradient of 5–90% HPLC buffer B for 53.5 min (0.1% formic acid in acetonitrile) on a home-packed C18 (Luna 5 µm, 100Å pores; Phenomenex) capillary reverse-phase HPLC

column (20 cm in length and 75 μm in internal diameter) with an integrated emission tip (New Objective, Inc.) and electrosprayed to the Orbitrap Fusion mass spectrometer (Thermo Fisher Scientific). The MS instrument was operated in a data-dependent mode with one full MS scan in Orbitrap at a resolution of 60,000 (200 m/z) followed by data-dependent MS/MS in linear ion trap with a stepped high-energy collision dissociation (HCD) at 35% and an isolation window of 1.2 m/z. LC–MS data were analyzed by MaxQuant software (version 1.5.3.12)[87] and searched against the protein sequence database of the target monoubiquitinated proteins ($\alpha Syn^{His}_{1–140}$ and $ALIX^{His}_{1–868*}$) concatenated with common contamination proteins. Trypsin and Glu-C were specified as proteolytic enzymes, acetylation on protein N-terminus, oxidation on methionine, heavy acetyl ($^{13}CD_3$-^{13}CO) modification on peptide N-terminus, Ac-GG modification on protein N-terminus, Ac-GG and heavy Ac($^{13}CD_3$-^{13}CO)-GG modification on lysine were specified as variable modifications and cysteine carbamidomethylation were specified as a fixed modification. False discovery rate of 1% with the target-decoy strategy was applied for all peptide and protein identifications. Peptides identified with Ac-GG labeling were manually analyzed using Xcalibur (version 4.1; Thermo Fisher Scientific) to quantify the heavy and light ubiquitinated peptide forms and ubiquitination stoichiometry as previously described.[81]

Fluorophore labeling.

$\alpha Syn^{His}_{1–140}$ was mixed with a 4-molar equivalent of ATTO-488 NHS ester in 20 mM sodium carbonate buffer (pH 8.3); total incubation time: ~1 h at room temperature. Unreacted dye was removed using a PD MidiTrap G-25 desalting column (Cytiva), and the buffer was exchanged to 25 mM Tris, pH 7.4, 50 mM NaCl, and 1 mM EDTA.

$ALIX^{His}_{1–868*}$ was mixed with 10-molar equivalents of Cy3 maleimide in 25 mM HEPES, pH 7.4, 150 mM NaCl, 1 mM tris(2-carboxyethyl)phosphine [TCEP], and 1 mM EDTA; total

incubation time: ~2 h at room temperature, followed by 4 °C overnight. Unreacted dye was removed using a PD MidiTrap G-25 desalting column.

Phase separation.

$\alpha Syn^{His}_{1–140}$ and its monoubiquitinated counterpart were dialyzed in 25 mM Tris, pH 7.4, 50 mM NaCl, and 1 mM EDTA. Phase separation was initiated by the addition of 10% (w/v) PEG-8000. In all samples, the protein concentration was maintained at 200 μM. For $ALIX^{His}_{1–868*}$, unmodified and monoubiquitinated proteins were dialyzed in 25 mM HEPES, pH 7, 150 mM NaCl, 1 mM DTT, and 1 mM EDTA. Phase separation was initiated by the addition of 5% (w/v) PEG-4000. In all samples, the protein concentration was maintained at 50 μM.

NMR.

Samples of ^{15}N-labeled or $^{15}N/^{13}C$-labeled ubiquitin variants, namely $Ub_{1–76}$, $Ub^{Strep(GS)_2}_{1–76}$, and $Ub^{(GS)_2}_{1–76}$, were prepared in a buffer comprising 20 mM sodium phosphate, pH 6.5, and 1 mM EDTA. A similar buffer composition with the addition of 1 mM TCEP was used for NMR titration experiments (see below). An aligned sample of ^{15}N-labeled $Ub^{Strep(GS)_2}_{1–76}$ was prepared using 5% PEG-hexanol.[88] All NMR samples contained 7% (v/v) deuterium oxide.

NMR experiments were carried out at 27 °C on Bruker 600 and 800 MHz spectrometers equipped with z-gradient triple resonance cryoprobes. Spectra were processed using NMRPipe[89] and analyzed using the CCPN software suite.[90] Sequential ^{1}H, ^{15}N, and ^{13}C backbone resonance assignments of ubiquitin variants were carried out using transverse relaxation optimized spectroscopy (TROSY)-based three-dimensional (3D) triple resonance experiments.[91] NMR chemical shift perturbation experiments were performed using 0.1 mM ^{15}N-labeled $Ub_{1–76}$ and unlabeled $ALIX_{348–702}$ / $ALIX^{His}_{1–868*}$ (0.1 mM each). Perturbations were calculated as follows: $\Delta_{H/N} = \{(\Delta\delta_{HN})^2 + (0.154 \times \Delta\delta_N)^2\}^{1/2}$, where $\Delta\delta_{HN}$ and $\Delta\delta_N$ are the $^{1}H_N$ and ^{15}N chemical shift

differences in ppm, respectively, between free and bound states. $^{1}D_{NH}$ residual dipolar couplings (RDCs), given by the difference in $^{1}J_{NH}$ coupling constants in aligned and isotropic media, were measured using the TROSY-based ARTSY technique[92] and analyzed with Xplor-NIH.[93]

Microscopy.

Glass coverslips (VWR; catalog no. 48366-172) were passivated[94] using the following protocol. Coverslips were heated and sonicated for 10 minutes in 1% Hellmanex III solution (Sigma-Aldrich, catalog no. Z805939). Coverslips were rinsed with 0.1 M NaOH and water. Cleaned coverslips were dried with nitrogen, rinsed with acetone, and dried again followed by the application of 5% (w/v) mPEG20K-Silane (Sigma-Aldrich, catalog no. JKA3100) in dimethyl sulfoxide. Coverslips were then incubated at 90 °C for 20 min. Passivated coverslips were rinsed with water and dried with nitrogen before use.

Condensate samples for differential interference contrast (DIC) microscopy were applied to passivated coverslips (see above) and incubated for 5 min at room temperature to allow condensates to settle onto the surface before being sandwiched by another passivated coverslip. DIC microscopy was performed on a Nikon Ti2 widefield microscope equipped with a DS-Qi2 CMOS camera and a 6x/1.4NA oil DIC N2 Objective. The samples were excited by a 470/555 nm laser controlled by a Lumencor SpectraX for imaging of ATTO-488, and Cy3, respectively.

Condensate samples for fluorescence recovery after photobleaching (FRAP) assays were applied to passivated coverslips with silicone gaskets (EMD-Millipore; catalog no. GBL664112) and allowed to incubate for 5 min at room temperature before sealing the gasket with an additional coverslip. FRAP experiments were performed on a Nikon point scanning confocal C2 with 2 GaAsP PMTs using a Plan Apo λ 60x/1.4 NA oil objective. Data collection consisted of two pre-photobleaching frames excited at 0.5% 488 nm laser power, followed by photobleaching with 2

iterations of 10% 488 nm laser power directed at the bleaching area for 4 s, and subsequently excited at 0.2% 488 nm laser power at 0.5 s intervals for 302 frames as post-photobleaching frames. Images were corrected for background fluorescence and intensity from the bleached region was normalized against the intensity of prebleached droplets.

Timelapse for the fusion of condensates of $\alpha Syn^{His}_{1–140}$ and its monoubiquitinated counterpart were performed at room temperature in 25 mM Tris, pH 7.4, 50 mM NaCl, 1 mM EDTA and 10% (w/v) PEG-8000, with 200 μM proteins (10% ATTO-488 labeled and 90% unlabeled). Images were collected every 60 s over the course of 142 minutes using a 488 nm laser on an EVOS M5000 (Thermo Fisher Scientific) using a Plan Apo λ 60x/1.4 NA oil objective (Olympus).

Thioflavin T (ThT) aggregation assays.

ThT aggregation assays of $\alpha Syn^{His}_{1–140}$ and its monoubiquitinated counterpart were performed in buffer containing 50 mM sodium acetate, pH 5.1, 1 mM EDTA, and 20 μM ThT (protein concentration = 30 μM). Samples were incubated at 37 °C in sealed 96-well flat bottom plates (Corning, catalog no. 3370) containing 100 μL sample per well (n = 2). Measurements were carried out with 3 min of orbital shaking (2 mm, 280 rpm) and 2 min of rest using a microplate reader (Infinite M Plex, Tecan). ThT fluorescence was recorded as a function of time (every 5 min); excitation and emission wavelengths were 415 and 480 nm, respectively.

Monoubiquitinated $ALIX^{His}_{1–868*}$ was allowed to aggregate for a few days to create seeds.[95] Seeds were resuspended in a buffer comprising 25 mM HEPES, 150 mM NaCl, 1 mM EDTA, and 1 mM DTT before addition to the solutions of fresh monoubiquitinated $ALIX^{His}_{1–868*}$ and its unmodified counterpart (100 μM each). Seeds represented ~5% of the total protein mass. ThT fluorescence

(20 μM) was recorded every 10 min with continuous shaking (the remaining parameters were same as above).

Transmission electron microscopy (TEM).

TEM samples of α-synuclein and ALIX fibrils were prepared using our published protocol.[96] TEM images were acquired using a JEM-1400Plus transmission electron microscope (JEOL) and recorded on a OneView digital camera (Gatan).

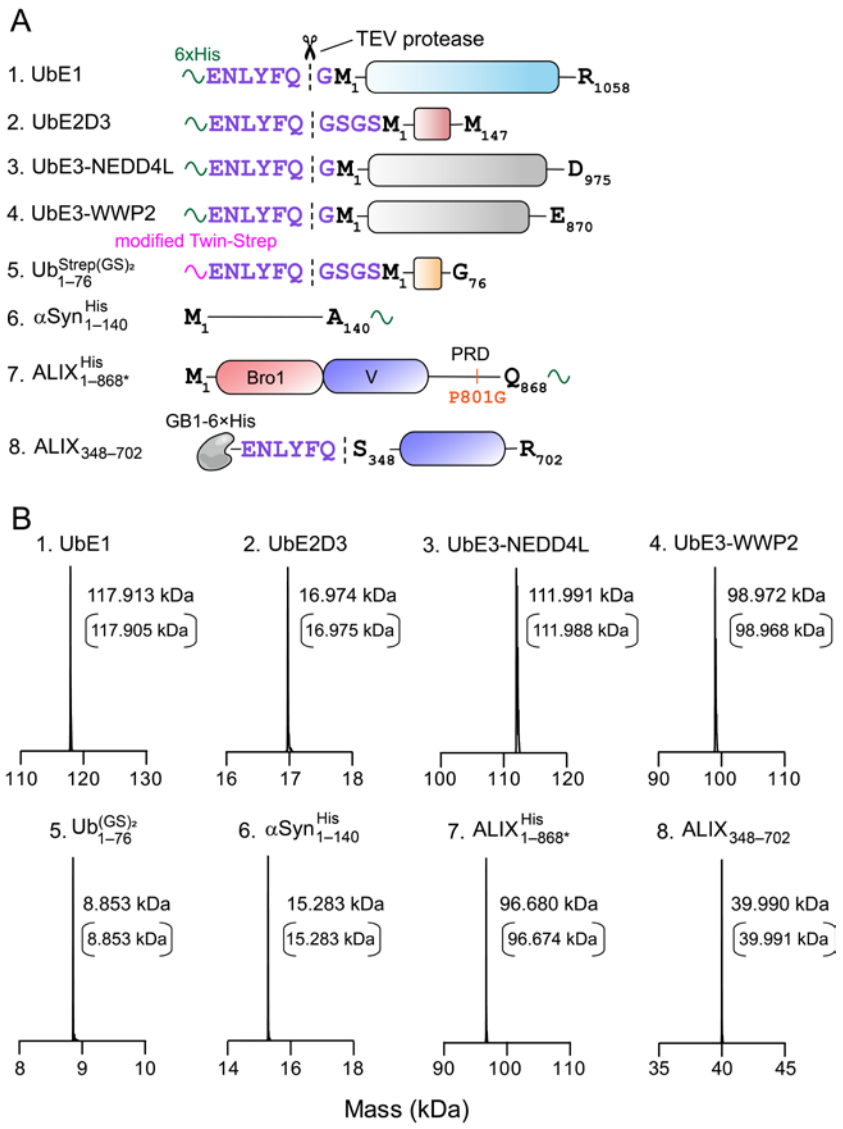

Figure 7 Recombinant constructs used in current study

(**A**) List of proteins used in current study. Each protein construct is designated by a number; see Table 1 for expression conditions, UniProt, and Addgene entries of each construct. All constructs were custom synthesized from Azenta Life Sciences. The native residues at the N- and C-termini of each construct are labeled in black. The primary sequences of TEV protease cleavage sites are labeled in purple. The locations of the TEV cleavage sites are marked by vertical dashed lines and scissors. 6xHis (green ribbon) denotes a polyhistidine affinity tag comprising six Figure 4 (con't). histidine residues. For $Ub_{1–76}^{Strep(GS)_2}$ (construct 5), the primary sequence of the modified twin-strep-tag is as follows: MGSWSHPQFE<u>R</u>(GGGS)$_2$GGS<u>S</u>AWSHPQFE<u>R</u>GS. This sequence differs from Schmidt and colleagues' original twin-strep-tag sequence[79] in the following two ways: (1) the bold and underlined arginine residues are mutated from the original sequence's lysine residues to prevent spurious ubiquitination, and (2) an extra serine residue (bold and underlined) was incorporated to increase bacterial expression. Both substrates, $\alpha Syn_{1–140}^{His}$ and $ALIX_{1–868*}^{His}$ (constructs 6 and 7, respectively), carry non-cleavable C-terminal 6xHis affinity tags. For $ALIX_{1–868*}^{His}$, the asterisk denotes the P801G point-mutation (orange) that was required for its overexpression in E. coli.[78] For $ALIX_{348–702}$ (construct 8), GB1–6xHis denotes protein GB1,[86] used to enhance protein expression levels, followed by a spacer sequence, and a polyhistidine affinity tag. (**B**) Analysis of TEV-cleaved recombinant proteins using liquid chromatography–electrospray ionization–time-of-flight mass spectrometry (LC–ESI–TOFMS); the numbers in parenthesis represent the corresponding theoretical masses.

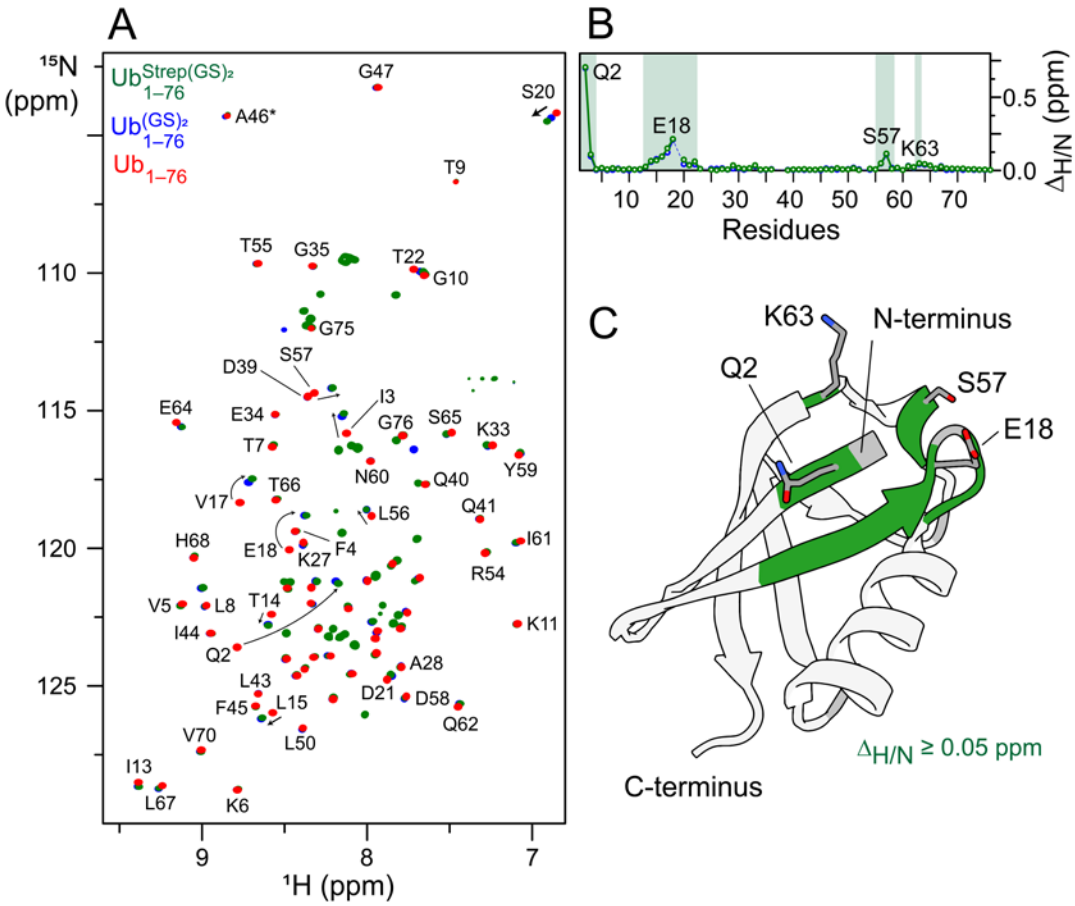

Figure 8 NMR chemical shift analysis of ubiquitin constructs used in current study

(**A**) Overlay of the expanded regions of $^{1}H–^{15}N$ TROSY–HSQC spectra of $Ub_{1–76}^{Strep(GS)_2}$, $Ub_{1–76}^{(GS)_2}$, and $Ub_{1–76}$ (green, blue, and red, respectively). A few of the $^{1}H–^{15}N$ cross-peaks of $Ub_{1–76}$ are labeled (folded cross-peaks of residue A46 are marked by an asterisk). The changes in chemical shifts of the $^{1}H–^{15}N$ cross-peaks due to the presence of the N-terminal modified twin-strep tag and/or GSGS linker remnant of the TEV cleavage site (cf. Fig. S1A) are marked by arrows. (**B**) $^{1}H_N/^{15}N$ chemical shift perturbation profiles of $Ub_{1–76}$ vs. $Ub_{1–76}^{Strep(GS)_2}$, and $Ub_{1–76}$ vs. $Ub_{1–76}^{(GS)_2}$ (green and blue, respectively). Semi-transparent green rectangles indicate residues (2–3, 14–22, 56–57, and 63) that exhibit large chemical shift perturbations (≥0.05 ppm). A few residues are labeled. (**C**) Ribbon diagram of ubiquitin (PDB entry: 1UBQ)[9]; a few of the residues that undergo large chemical shift changes due to N-terminal modifications (i.e., modified twin-strep tag and/or GSGS linker) are shown in stick representation. Green ribbons represent residues that are most affected ($\Delta_{H/N} \geq 0.05$ ppm). Grey ribbons represent residues that could not be assigned unambiguously and the N-terminal methionine. The experimental data were recorded at 27 °C and a spectrometer ^{1}H frequency of 600 MHz

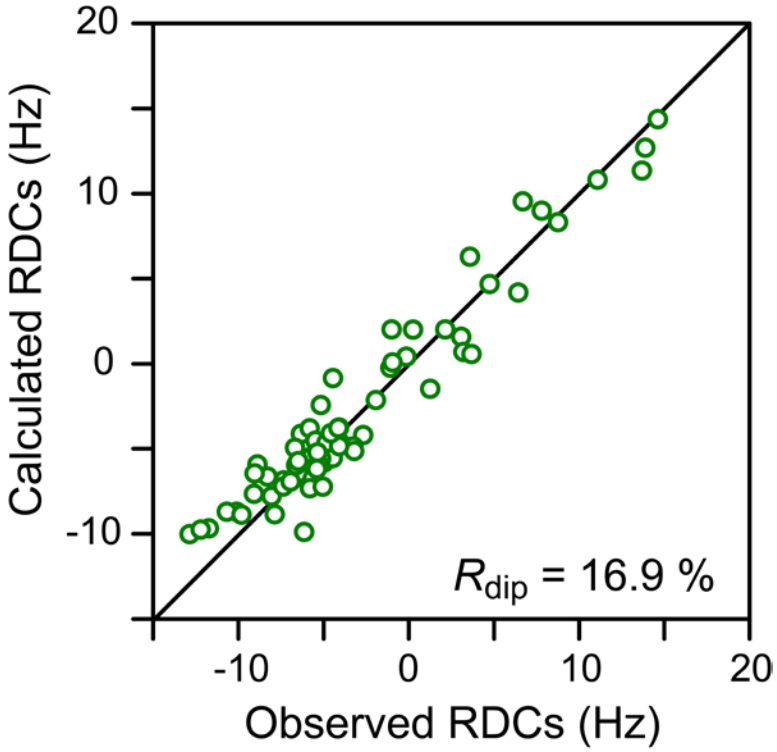

Figure 9 Backbone RDC analysis of $Ub_{1-76}^{Strep(GS)_2}$

Singular value decomposition (SVD) analysis showing agreement of the experimental backbone amide ($^1D_{NH}$) RDCs acquired in 5% PEG-hexanol with those calculated from the X-ray coordinates of ubiquitin (PDB entry: 1UBQ)[9]. Only residues in secondary structure elements are used for the SVD fit. The RDC R-factor, R_{dip}, is given by $\{<(D_{obs}-D_{calc})^2>/(2<D_{obs}^2>)\}^{1/2}$, where D_{obs} and D_{calc} are the observed and calculated $^1D_{NH}$ RDC values, respectively.[97] Excellent agreement between observed and calculated RDC values with R_{dip} of ~17% indicate that $Ub_{1-76}^{Strep(GS)_2}$ adopts the same fold in solution as that of wild-type ubiquitin. The experimental data were recorded at 27 °C and a spectrometer ^1H frequency of 800 MHz. The concentrations of proteins in aligned and isotropic samples were 0.2 mM each.

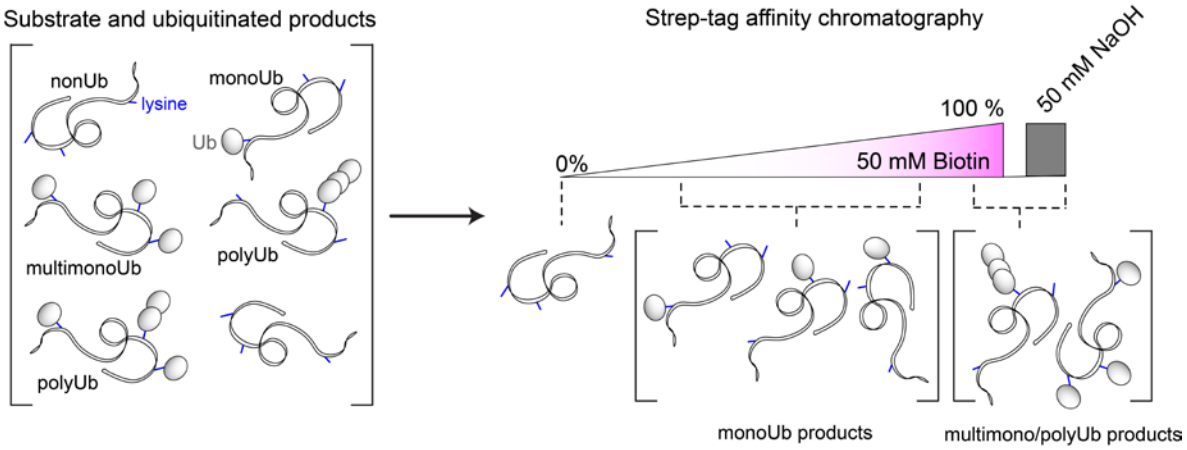

Figure 10 Exploiting the avidity effect for the selective purification of monoubiquitinated species

Reaction components from Step-3 (see Fig. 4A, main text) comprising substrate and its ubiquitinated products were subjected to Strep-tag affinity chromatography. Components carrying a single $Ub_{1-76}^{Strep(GS)_2}$ molecule comprising a modified twin-strep tag, i.e., monoubiquitinated products, bound efficiently to the tetrameric strep-tactin, a derivative of streptavidin. These monoubiquitinated species could, however, be readily displaced from the resin-coupled strep-tactin by biotin. In contrast, components carrying two or more $Ub_{1-76}^{Strep(GS)_2}$ molecules, namely multi-mono- and poly-ubiquitinated products, remained tightly bound to the resin due to the avidity effect and could only be displaced using 50 mM biotin or 50 mM sodium hydroxide (the latter was used to regenerate the resin for the next use). The avidity effect, which we define as the increased strength of binding due to multiple interactions, likely originates from the simultaneous binding of multiple twin-strep tags of multi-mono- and poly-ubiquitinated products to the tetrameric strep-tactin.

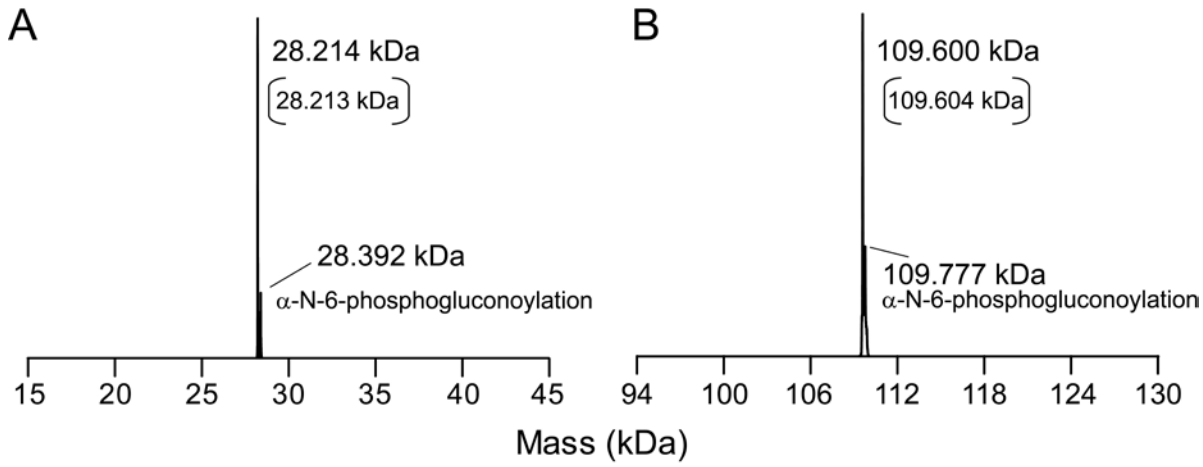

Figure 11 Mass-spectrometry analysis of monoubiquitinated α-synuclein and ALIX

LC–ESI–TOFMS analyses of monoubiquitinated (**A**) αSyn^{His}_{1-140} and (**B**) $ALIX^{His}_{1-868*}$. NEDD4L and WWP2 were used for monoubiquitination of α-synuclein and ALIX, respectively. Also see Fig. 1B–C (main text) for the corresponding western blots and SDS-PAGE gel analyses. The numbers in parenthesis represent theoretical masses calculated using the formula: mass of intact $Ub^{Strep(GS)_2}_{1-76}$ (12.948 kDa; note that Fig. S1B reports the mass of TEV-cleaved $Ub^{(GS)_2}_{1-76}$) + mass of the substrate (15.283 kDa for αSyn^{His}_{1-140} / 96.674 kDa for $ALIX^{His}_{1-868*}$) – 0.018 kDa (representing the loss of water molecule owing to the formation of the isopeptide bond). Minor peaks (representing approximately 178 Da addition) are most likely caused by α-N-6-phosphogluconoylation[98] of the modified twin-strep tag of $Ub^{Strep(GS)_2}_{1-76}$.

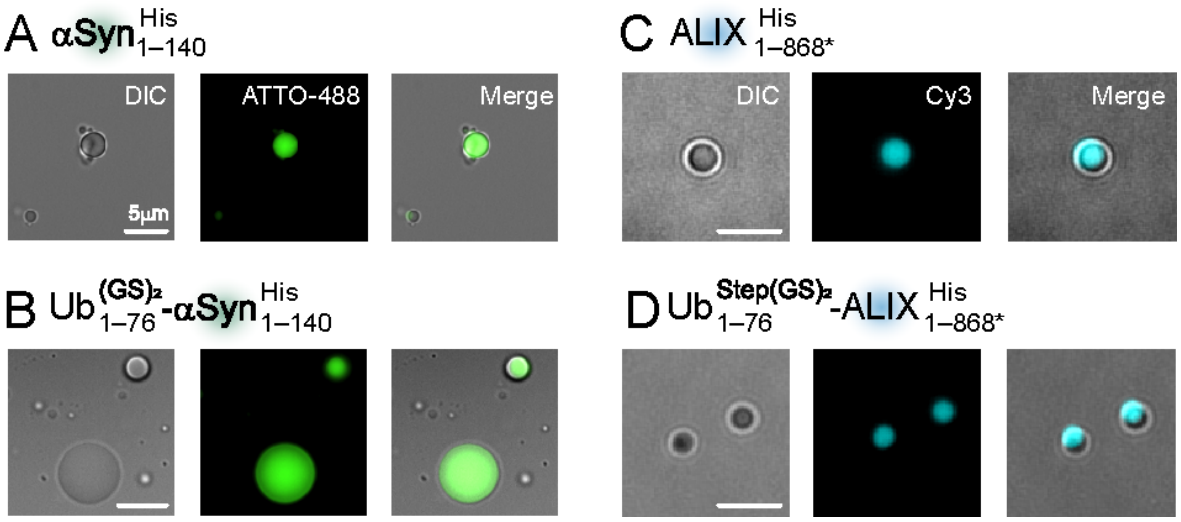

Figure 12 Phase separation of α-synuclein and ALIX and the impact of monoubiquitination

Representative microscopy images of condensates formed by ATTO-488 labeled (A) $\alpha Syn^{His}_{1–140}$ and (B) its monoubiquitinated counterpart, and Cy3-labeled (C) $ALIX^{His}_{1–868*}$ and (D) its monoubiquitinated species. NEDD4L and WWP2 were used for monoubiquitination of α-synuclein and ALIX, respectively. Phase separation experiments for α-synuclein were performed at room temperature in 25 mM Tris, pH 7.4, 50 mM NaCl, 1 mM EDTA and 10% (w/v) PEG-8000, with 200 µM protein. For ALIX, experiments were performed at room temperature in 25 mM HEPES, pH 7.4, 150 mM NaCl, 1 mM DTT, 1 mM EDTA, and 5% (w/v) PEG-4000, with 50 µM protein. All fluorescently labeled droplets were prepared using 10% labeled and 90% unlabeled protein. Images were taken immediately after the formation of condensates.

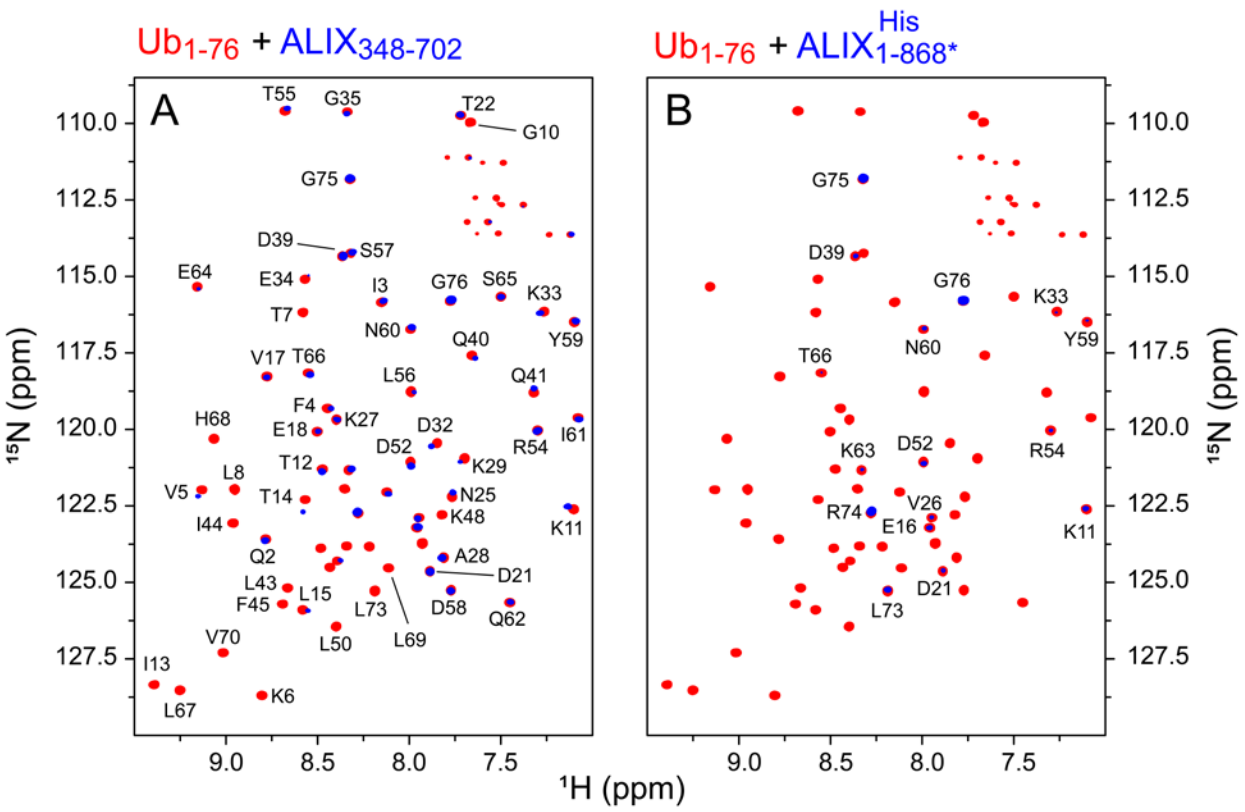

Figure 13 NMR analyses of ubiquitin–ALIX interactions

Expanded regions of ^{1}H-^{15}N TROSY-HSQC spectra of 100 µM ^{15}N-labeled Ub_{1-76}, in the absence (red) and presence (blue) of its non-labeled binding partners (100 µM each), namely (**A**) the V-domain of ALIX, $ALIX_{348–702}$, and (**B**) full-length ALIX, $ALIX^{His}_{1–868*}$. A few isolated ^{1}H–^{15}N cross-peaks are labeled. All spectra were recorded at a spectrometer ^{1}H frequency of 800 MHz. The experimental conditions were as follows: 20 mM sodium phosphate, pH 6.5, 1 mM EDTA, and 1 mM TCEP at 27 °C.

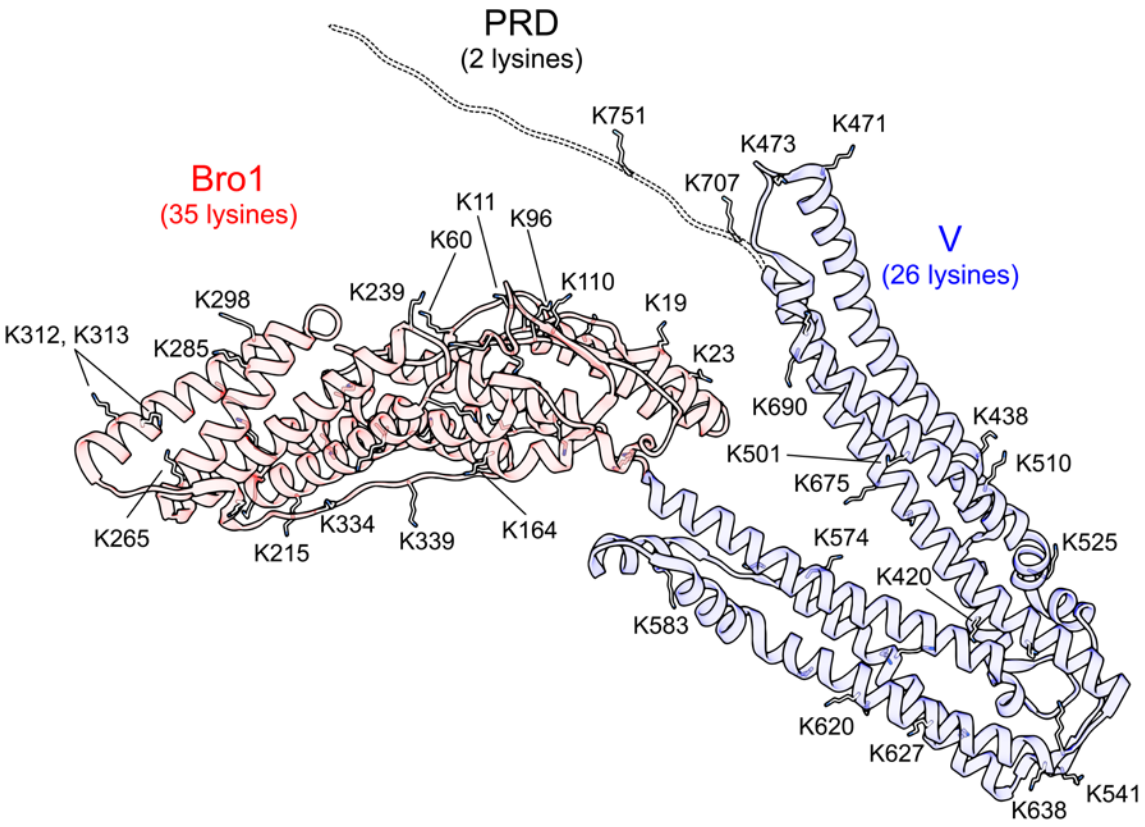

Figure 14 ALIX and the location of its lysine residues

Schematic of ALIX comprising Bro1, V, and PRD (red and blue ribbons and dashed black lines, respectively), derived from the X-ray structure of Bro1-V domains (PDB entry: 2XS1).[63] Note that unlike Bro1 and V domains, the structure of PRD is not available as it is disordered.[59] The lysine residues of ALIX are shown in stick representation. A few of the isolated residues are labeled.

Table 1 Recombinant constructs used in current study

Construct	UniProt entry	Addgene Accession no.	Competent cells[a]	Induction temperature[b]	Growth medium[c]	Yield (mg/1L)[d]
UbE1	P22314	186804	BL21-AI	16 °C	TB	10 mg
UBE2D3	P61077	186805	BL21-AI	16 °C	TB	100 mg
NEDD4L	Q96PU5	186806	BL21-AI	16 °C	TB	20 mg
WWP2	O00308	186807	BL21-AI	16 °C	TB	15 mg
$Ub_{1-76}^{Strep(GS)2}$	P0CG48	186803	BL21(DE3)	16 °C	LB	12 mg
αSyn_{1-140}^{His}	P37840	186802	BL21-AI	37 °C	LB	20 mg
$ALIX_{1-868*}^{His}$	Q8WUM4	186808	BL21-AI	16 °C	LB	30 mg
$ALIX_{348–702}$	Q8WUM4	189819	BL21-(DE3)	16 °C	LB	40 mg

a) BL21(DE3) and BL21-AI cells were obtained from Agilent (catalog no. 200131) and Thermo Fisher Scientific (catalog no. C607003), respectively.

b) Cultures were grown overnight upon induction with 1 mM IPTG (and 0.2% w/v arabinose; the latter was used for BL21-AI cells).

c) TB broth and LB capsules were obtained from Thermo Fischer Scientific (catalog no. BP9728-500) and MP Biomedicals (catalog no. 3002-036), respectively, and were used according to the manufacturers' protocols.

d) The yield represents total protein obtained from a liter of bacterial culture. In the case of ubiquitinating enzymes, $Ub_{1–76}^{Strep(GS)_2}$, and $ALIX_{348–702}$, it represents the total amount of protein obtained after cleaving off the N-terminal purification tag by TEV protease.

Table 2 Components of in vitro ubiquitination reactions and the yields of corresponding monoubiquitinated products[a,b]

Reaction Component	αSyn^{His}_{1-140} (250 μM)	$ALIX^{His}_{1-868*}$ (150 μM)	$ALIX^{His}_{1-868*}$ (150 μM)
UbE1	15 μM	15 μM	15 μM
UBE2D3	20 μM	20 μM	20 μM
NEDD4L	25 μM	—	25 μM
WWP2	—	25 μM	—
$Ub^{Strep(GS)2}_{1-76}$	500 μM	500 μM	500 μM
Monoubiquitinated product	2.5 mg / 5 mL	1.3 mg / 4 mL	1.2 mg / 4 mL

a) All reaction components were mixed, and the corresponding mixture was dialyzed against the buffer containing 50 mM Tris, pH 7.5, 1 mM DTT, 1 mM $MgCl_2$, and 1.5 mM ATP for 5 h at 30 °C.

b) In vitro ubiquitination reaction of $\alpha Syn^{His}_{1–140}$ + WWP2 was not performed as unlike ALIX, WWP2 has not been shown to ubiquitinate α-synuclein in vivo

Table 3 Quantification of the site-specific frequency of monoubiquitination for $\alpha Syn^{His}_{1\text{-}140}$ and $ALIX^{His}_{1\text{-}868*}$ using a chemical proteomics approach[a,b,c]

	NEDD4L		WWP2	
Lysine Residues	Average Stoichiometry	Percent Stoichiometry	Average Stoichiometry	Percent Stoichiometry
		$\alpha Syn^{His}_{1\text{-}140}$		
K6/K10/K12	2.14	18.69	—	—
K21/K23	1.17	10.19	—	—
K32/K34	0.03	0.28	—	—
K43/K45	0.51	4.48	—	—
K58/K60	0.37	3.20	—	—
K80	2.45	21.35	—	—
K96/K97/K102	4.79	41.81	—	—
		$ALIX^{His}_{1\text{-}868*}$		
K10/K11	0.06	0.07	0.53	0.77
K19/K23	1.29	1.52	1.04	1.53
K48	0.22	0.26	0.12	0.17
K60	0.78	0.92	1.37	2.01
K81	—	—	—	—
K96	—	—	—	—
K101	—	—	—	—
K110	—	—	—	—
K120	—	—	—	—
K147	—	—	—	—
K151	—	—	—	—
K164	—	—	—	—
K202	0.18	0.21	0.16	0.24

Table S3 (cont'd).

Lysine Residues	NEDD4L Average Stoichiometry	NEDD4L Percent Stoichiometry	WWP2 Average Stoichiometry	WWP2 Percent Stoichiometry
		$ALIX^{His}_{1\text{-}868*}$		
K207	—	—	—	—
K209	—	—	—	—
K215	—	—	—	—
K229	—	—	—	—
K234	—	—	—	—
K239	—	—	—	—
K248	2.44	2.88	2.98	4.39
K265	1.42	1.68	2.56	3.76
K268/K269	0.83	0.98	0.63	0.92
K285	0.64	0.75	0.58	0.85
K298/K303	0.69	0.82	0.84	1.24
K312/K313	0.25	0.30	0.24	0.36
K327	—	—	—	—
K334	—	—	—	—
K339	—	—	—	—
K350	—	—	—	—
K357	0.51	0.60	0.41	0.60
K374	0.19	0.23	0.21	0.32
K420	10.98	12.95	17.44	25.67
K438	1.85	2.19	2.22	3.27
K471/K473	1.47	1.74	2.37	3.48
K486	0.32	0.38	0.36	0.53
K501/K510	32.36	38.16	5.41	7.97
K525	2.03	2.39	0.72	1.06
K541	3.49	4.12	0.27	0.39

Table S3 (cont'd).

Lysine Residues	NEDD4L Average Stoichiometry	NEDD4L Percent Stoichiometry	WWP2 Average Stoichiometry	WWP2 Percent Stoichiometry
		$ALIX^{His}_{1\text{-}868*}$		
K553/K563/K564	0.28	0.33	0.63	0.93
K574	—	—	—	—
K583	0.00	0.00	0.00	0.00
K614	0.25	0.30	0.24	0.35
K620/K621	0.09	0.11	0.02	0.02
K627	0.69	0.81	0.90	1.33
K638/K640	6.08	7.16	7.74	11.39
K654	1.42	1.67	1.34	1.97
K671	0.48	0.57	0.25	0.37
K675	0.03	0.03	0.17	0.26
K690	0.95	1.12	0.82	1.21
K699/K707	4.47	5.27	4.21	6.19
K751	8.04	9.48	11.18	16.46

a) Stoichiometry was determined by dividing the precursor ion LC-MS chromatographic peak area of a monoubiquitinated peptide by the sum of the peak areas of the peptide's mono- and non-ubiquitinated forms. Two independent reactions were used to calculate the averages.

b) Percentages were calculated by summing the average stoichiometries, which represented the total pool of monoubiquitinated species.

c) In vitro ubiquitination reaction of $\alpha Syn^{His}_{1\text{–}140}$ + WWP2 was not performed as unlike ALIX, WWP2 has not been shown to ubiquitinate α-synuclein in vivo.

Associated content

Human UbE1 (UniProt accession no. P22314), UbE2D3 (UniProt accession no. P61077), NEDD4L (UniProt accession no. Q96PU5), WWP2 (UniProt accession no. O00308), ubiquitin (UniProt accession no. P0CG48), α-synuclein (UniProt accession no. P37840), and ALIX (UniProt accession no. Q8WUM4). The constructs of $Ub_{1–76}^{Strep(GS)_2}$, UbE1, UbE2D3, NEDD4L, WWP2, $ALIX_{1–868*}^{His}$, $ALIX_{348–702}$, and $\alpha Syn_{1–140}^{His}$ have been deposited in the Addgene repository as accession numbers 186803, 186804, 186805, 186806, 186807, 186808, 189819, and 186802, respectively. The NMR chemical shift assignments of $Ub_{1–76}^{Strep(GS)_2}$ have been deposited in the Biological Magnetic Resonance Bank as entry 51647. The mass spectrometry proteomics data have been deposited to the ProteomeXchange Consortium via the PRIDE partner repository as entry PXD037416.

Acknowledgements

Chapter 1, in full, has been submitted for publication of the material as it may appear in the Journal of the American Chemical Society, 2022, Nelson Spencer; Li, Yunan; Chen, Yue; Deshmukh, Lalit. “Avidity-based method for the efficient generation of monoubiquitinated recombinant proteins”. The -author of the thesis was the primary researcher and author of this paper.

CONCLUSION

Monoubiquitination is an important reversible posttranslational modification that controls a variety of cellular processes. While existing chemical methods can produce monoubiquitinated proteins, these methods are technically challenging, suffer from poor yields, and are thus not universally applicable. Here we present a novel method that produces milligram quantities of isopeptide-linked monoubiquitinated recombinant proteins using native enzymes. This method was applied to two amyloidogenic proteins, α-synuclein and ALIX. Using NEDD4-family ligases NEDD4L and WWP2, we generated monoubiquitinated forms of α-synuclein and ALIX. We discovered that monoubiquitination of α-synuclein and ALIX is site-specific, with most of the ubiquitination occurring at the C-terminal lysine residues of α-synuclein and the ALIX V-domain. Additionally, we identified site-specific differences in NEDD4L and WWP2-mediated monoubiquitination of ALIX. Furthermore, ubiquitination of α-synuclein and ALIX resulted in strikingly different behaviors in terms of their phase separation and fibrilization. Ubiquitinated α-synuclein condensates were dynamic and retained their liquid-like properties when compared to condensates of unmodified α-synuclein. In contrast, the condensates of monoubiquitinated ALIX were rigid and nondynamic. While α-synuclein formed amyloid fibrils, its monoubiquitinated form formed amorphous aggregates. This contrasts with ALIX, which could not form fibrils on its own but, upon monoubiquitination, could produce fibrillar structures. Collectively, these results demonstrate the impact of monoubiquitination on the biophysical properties of these two proteins. Our method can aid in identifying biologically relevant ubiquitination sites. It can also be used in conjunction with site-specific ubiquitination methods to compare heterogeneous and homogeneous ubiquitinated proteins, providing insight into potential differences between bulk

ubiquitinated and site-specific ubiquitinated proteins. We anticipate that the ease of use of our method will allow its adoption by other laboratories and will greatly hasten further studies of protein monoubiquitination.

REFERENCES

1. Braten, O.; Livneh, I.; Ziv, T.; Admon, A.; Kehat, I.; Caspi, L. H.; Gonen, H.; Bercovich, B.; Godzik, A.; Jahandideh, S.; Jaroszewski, L.; Sommer, T.; Kwon, Y. T.; Guharoy, M.; Tompa, P.; Ciechanover, A., Numerous proteins with unique characteristics are degraded by the 26S proteasome following monoubiquitination. *Proc. Natl. Acad. Sci. U.S.A.* **2016,** *113* (32), E4639-E4647.

2. Schwertman, P.; Bekker-Jensen, S.; Mailand, N., Regulation of DNA double-strand break repair by ubiquitin and ubiquitin-like modifiers. *Nat. Rev. Mol. Cell Biol.* **2016,** *17* (6), 379-394.

3. Sette, P.; Nagashima, K.; Piper, R. C.; Bouamr, F., Ubiquitin conjugation to Gag is essential for ESCRT-mediated HIV-1 budding. *Retrovirology* **2013,** *10* (1), 79.

4. Ren, X.; Hurley, J. H., VHS domains of ESCRT-0 cooperate in high-avidity binding to polyubiquitinated cargo. *EMBO J.* **2010,** *29* (6), 1045-54.

5. Henne, W. M.; Buchkovich, N. J.; Emr, S. D., The ESCRT pathway. *Dev. Cell* **2011,** *21* (1), 77-91.

6. Groen, E. J. N.; Gillingwater, T. H., UBA1: At the crossroads of ubiquitin homeostasis and neurodegeneration. *Trends Mol. Med.* **2015,** *21* (10), 622-632.

7. Metzger, M. B.; Hristova, V. A.; Weissman, A. M., HECT and RING finger families of E3 ubiquitin ligases at a glance. *J. Cell Sci.* **2012,** *125* (Pt 3), 531-7.

8. Akutsu, M.; Dikic, I.; Bremm, A., Ubiquitin chain diversity at a glance. *J. Cell Sci.* **2016,** *129* (5), 875-80.

9. Vijay-Kumar, S.; Bugg, C. E.; Cook, W. J., Structure of ubiquitin refined at 1.8 Å resolution. *J. Mol. Biol.* **1987,** *194* (3), 531-44.

10. Komander, D.; Rape, M., The ubiquitin code. *Annu. Rev. Biochem.* **2012,** *81*, 203-29.

11. Dikic, I.; Wakatsuki, S.; Walters, K. J., Ubiquitin-binding domains — from structures to functions. *Nat. Rev. Mol. Cell Biol.* **2009,** *10* (10), 659-671.

12. Keren-Kaplan, T.; Attali, I.; Estrin, M.; Kuo, L. S.; Farkash, E.; Jerabek-Willemsen, M.; Blutraich, N.; Artzi, S.; Peri, A.; Freed, E. O.; Wolfson, H. J.; Prag, G., Structure-based in silico identification of ubiquitin-binding domains provides insights into the ALIX-V:ubiquitin complex and retrovirus budding. *EMBO J.* **2013,** *32* (4), 538-51.

13. Csizmadia, T.; Lőw, P., The role of deubiquitinating enzymes in the various forms of autophagy. *Int. J. Mol. Sci.* **2020,** *21* (12).

14. Kaiser, S. E.; Riley, B. E.; Shaler, T. A.; Trevino, R. S.; Becker, C. H.; Schulman, H.; Kopito, R. R., Protein standard absolute quantification (PSAQ) method for the measurement of cellular ubiquitin pools. *Nat. Methods* **2011,** *8* (8), 691-6.

15. Chen, Y.; Zhou, D.; Yao, Y.; Sun, Y.; Yao, F.; Ma, L., Monoubiquitination in homeostasis and cancer. *Int. J. Mol. Sci.* **2022,** *23* (11), 5925.

16. Holding, C., How ubiquitin silences genes. *Genome Biol.* **2004,** *5* (1), 9000.

17. Minsky, N.; Shema, E.; Field, Y.; Schuster, M.; Segal, E.; Oren, M., Monoubiquitinated H2B is associated with the transcribed region of highly expressed genes in human cells. *Nat. Cell Biol.* **2008,** *10* (4), 483-488.

18. Greer, S. F.; Zika, E.; Conti, B.; Zhu, X. S.; Ting, J. P., Enhancement of CIITA transcriptional function by ubiquitin. *Nat. Immunol.* **2003,** *4* (11), 1074-82.

19. He, H.; Peng, Y.; Fan, S.; Chen, Y.; Zheng, X.; Li, C., Cullin3/KCTD5 induces monoubiquitination of ΔNp63α and impairs its activity. *FEBS Lett.* **2018,** *592* (13), 2334-2340.

20. Waterman, H.; Yarden, Y., Molecular mechanisms underlying endocytosis and sorting of ErbB receptor tyrosine kinases. *FEBS Lett.* **2001,** *490* (3), 142-52.

21. Isasa, M.; Katz, E. J.; Kim, W.; Yugo, V.; González, S.; Kirkpatrick, D. S.; Thomson, T. M.; Finley, D.; Gygi, S. P.; Crosas, B., Monoubiquitination of RPN10 regulates substrate recruitment to the proteasome. *Mol. Cell* **2010,** *38* (5), 733-45.

22. Rott, R.; Szargel, R.; Haskin, J.; Shani, V.; Shainskaya, A.; Manov, I.; Liani, E.; Avraham, E.; Engelender, S., Monoubiquitylation of alpha-synuclein by seven in absentia homolog (SIAH) promotes its aggregation in dopaminergic cells. *J. Biol. Chem.* **2008,** *283* (6), 3316-3328.

23. Ham, S. J.; Lee, D.; Yoo, H.; Jun, K.; Shin, H.; Chung, J., Decision between mitophagy and apoptosis by Parkin via VDAC1 ubiquitination. *Proc. Natl. Acad. Sci. U.S.A.* **2020,** *117* (8), 4281-4291.

24. Kim, M. O.; Chawla, P.; Overland, R. P.; Xia, E.; Sadri-Vakili, G.; Cha, J. H., Altered histone monoubiquitylation mediated by mutant huntingtin induces transcriptional dysregulation. *J. Neurosci.* **2008,** *28* (15), 3947-57.

25. Tan, W.; van Twest, S.; Leis, A.; Bythell-Douglas, R.; Murphy, V. J.; Sharp, M.; Parker, M. W.; Crismani, W.; Deans, A. J., Monoubiquitination by the human Fanconi anemia core complex clamps FANCI:FANCD2 on DNA in filamentous arrays. *Elife* **2020,** *9*.

26. Tsui, V.; Crismani, W., The Fanconi anemia pathway and fertility. *Trends Genet.* **2019,** *35* (3), 199-214.

27. Votteler, J.; Sundquist, W. I., Virus budding and the ESCRT pathway. *Cell Host Microbe* **2013,** *14* (3), 232-41.

28. Stanley, M.; Virdee, S., Chemical ubiquitination for decrypting a cellular code. *Biochem. J.* **2016,** *473* (10), 1297-314.

29. Koga, S.; Sekiya, H.; Kondru, N.; Ross, O. A.; Dickson, D. W., Neuropathology and molecular diagnosis of Synucleinopathies. *Mol. Neurodegener.* **2021,** *16* (1), 83.

30. de Oliveira, G. A. P.; Silva, J. L., Alpha-synuclein stepwise aggregation reveals features of an early onset mutation in Parkinson's disease. *Commun. Biol.* **2019,** *2* (1), 374.

31. Rott, R.; Szargel, R.; Haskin, J.; Bandopadhyay, R.; Lees, A. J.; Shani, V.; Engelender, S., α-Synuclein fate is determined by USP9X-regulated monoubiquitination. *Proc. Natl. Acad. Sci. U.S.A.* **2011,** *108* (46), 18666-71.

32. Abeywardana, T.; Lin, Y. H.; Rott, R.; Engelender, S.; Pratt, M. R., Site-specific differences in proteasome-dependent degradation of monoubiquitinated α-synuclein. *Chem. Biol.* **2013,** *20* (10), 1207-13.

33. Martinez-Vicente, M.; Vila, M., Alpha-synuclein and protein degradation pathways in Parkinson's disease: a pathological feed-back loop. *Exp. Neurol.* **2013,** *247*, 308-13.

34. Snyder, H.; Mensah, K.; Theisler, C.; Lee, J.; Matouschek, A.; Wolozin, B., Aggregated and monomeric alpha-synuclein bind to the S6' proteasomal protein and inhibit proteasomal function. *J Biol Chem* **2003,** *278* (14), 11753-9.

35. Emmanouilidou, E.; Stefanis, L.; Vekrellis, K., Cell-produced α-synuclein oligomers are targeted to, and impair, the 26S proteasome. *Neurobiol. Aging* **2010,** *31* (6), 953-968.

36. Cuervo, A. M.; Stefanis, L.; Fredenburg, R.; Lansbury, P. T.; Sulzer, D., Impaired degradation of mutant alpha-synuclein by chaperone-mediated autophagy. *Science* **2004,** *305* (5688), 1292-5.

37. Tofaris, G. K.; Kim, H. T.; Hourez, R.; Jung, J. W.; Kim, K. P.; Goldberg, A. L., Ubiquitin ligase Nedd4 promotes alpha-synuclein degradation by the endosomal-lysosomal pathway. *Proc Natl Acad Sci U S A* **2011,** *108* (41), 17004-9.

38. Ebrahimi-Fakhari, D.; McLean, P. J.; Unni, V. K., Alpha-synuclein's degradation in vivo: opening a new (cranial) window on the roles of degradation pathways in Parkinson disease. *Autophagy* **2012,** *8* (2), 281-3.

39. Nonaka, T.; Iwatsubo, T.; Hasegawa, M., Ubiquitination of alpha-synuclein. *Biochemistry* **2005,** *44* (1), 361-8.

40. Manzanza, N. O.; Sedlackova, L.; Kalaria, R. N., Alpha-synuclein post-translational modifications: implications for pathogenesis of Lewy body disorders. *Front Aging Neurosci.* **2021,** *13*, 690293.

41. Paleologou, K. E.; Oueslati, A.; Shakked, G.; Rospigliosi, C. C.; Kim, H. Y.; Lamberto, G. R.; Fernandez, C. O.; Schmid, A.; Chegini, F.; Gai, W. P.; Chiappe, D.; Moniatte, M.; Schneider, B. L.; Aebischer, P.; Eliezer, D.; Zweckstetter, M.; Masliah, E.; Lashuel, H. A., Phosphorylation at S87 is enhanced in synucleinopathies, inhibits alpha-synuclein oligomerization, and influences synuclein-membrane interactions. *J. Neurosci.* **2010,** *30* (9), 3184-98.

42. Feany, M. B.; Bender, W. W., A Drosophila model of Parkinson's disease. *Nature* **2000,** *404* (6776), 394-8.

43. Souza, J. M.; Giasson, B. I.; Chen, Q.; Lee, V. M.; Ischiropoulos, H., Dityrosine cross-linking promotes formation of stable alpha -synuclein polymers. Implication of nitrative and oxidative stress in the pathogenesis of neurodegenerative synucleinopathies. *J. Biol. Chem.* **2000,** *275* (24), 18344-9.

44. Hodara, R.; Norris, E. H.; Giasson, B. I.; Mishizen-Eberz, A. J.; Lynch, D. R.; Lee, V. M.; Ischiropoulos, H., Functional consequences of alpha-synuclein tyrosine nitration: diminished binding to lipid vesicles and increased fibril formation. *J. Biol. Chem.* **2004,** *279* (46), 47746-53.

45. Levine, P. M.; Galesic, A.; Balana, A. T.; Mahul-Mellier, A. L.; Navarro, M. X.; De Leon, C. A.; Lashuel, H. A.; Pratt, M. R., α-Synuclein O-GlcNAcylation alters aggregation and toxicity, revealing certain residues as potential inhibitors of Parkinson's disease. *Proc. Natl. Acad. Sci. U.S.A.* **2019,** *116* (5), 1511-1519.

46. Vicente Miranda, H.; Szego É, M.; Oliveira, L. M. A.; Breda, C.; Darendelioglu, E.; de Oliveira, R. M.; Ferreira, D. G.; Gomes, M. A.; Rott, R.; Oliveira, M.; Munari, F.; Enguita, F. J.; Simões, T.; Rodrigues, E. F.; Heinrich, M.; Martins, I. C.; Zamolo, I.; Riess, O.; Cordeiro, C.; Ponces-Freire, A.; Lashuel, H. A.; Santos, N. C.; Lopes, L. V.; Xiang, W.; Jovin, T. M.; Penque, D.; Engelender, S.; Zweckstetter, M.; Klucken, J.; Giorgini, F.; Quintas, A.; Outeiro, T. F., Glycation potentiates α-synuclein-associated neurodegeneration in synucleinopathies. *Brain* **2017,** *140* (5), 1399-1419.

47. Tofaris, G. K.; Razzaq, A.; Ghetti, B.; Lilley, K. S.; Spillantini, M. G., Ubiquitination of alpha-synuclein in Lewy bodies is a pathological event not associated with impairment of proteasome function. *J. Biol. Chem.* **2003,** *278* (45), 44405-11.

48. Engelender, S., Ubiquitination of alpha-synuclein and autophagy in Parkinson's disease. *Autophagy* **2008,** *4* (3), 372-4.

49. Shimura, H.; Schlossmacher, M. G.; Hattori, N.; Frosch, M. P.; Trockenbacher, A.; Schneider, R.; Mizuno, Y.; Kosik, K. S.; Selkoe, D. J., Ubiquitination of a new form of alpha-synuclein by parkin from human brain: implications for Parkinson's disease. *Science* **2001,** *293* (5528), 263-9.

50. Mund, T.; Masuda-Suzukake, M.; Goedert, M.; Pelham, H. R., Ubiquitination of alpha-synuclein filaments by NEDD4 ligases. *PLoS One* **2018,** *13* (7), e0200763.

51. Davies, S. E.; Hallett, P. J.; Moens, T.; Smith, G.; Mangano, E.; Kim, H. T.; Goldberg, A. L.; Liu, J. L.; Isacson, O.; Tofaris, G. K., Enhanced ubiquitin-dependent degradation by NEDD4 protects against α-synuclein accumulation and toxicity in animal models of Parkinson's disease. *Neurobiol. Dis.* **2014,** *64* (100), 79-87.

52. Meier, F.; Abeywardana, T.; Dhall, A.; Marotta, N. P.; Varkey, J.; Langen, R.; Chatterjee, C.; Pratt, M. R., Semisynthetic, site-specific ubiquitin modification of α-synuclein reveals differential effects on aggregation. *J. Am. Chem. Soc.* **2012,** *134* (12), 5468-71.

53. Haj-Yahya, M.; Fauvet, B.; Herman-Bachinsky, Y.; Hejjaoui, M.; Bavikar, S. N.; Karthikeyan, S. V.; Ciechanover, A.; Lashuel, H. A.; Brik, A., Synthetic polyubiquitinated α-Synuclein reveals important insights into the roles of the ubiquitin chain in regulating its pathophysiology. *Proc. Natl. Acad. Sci. U.S.A.* **2013,** *110* (44), 17726-31.

54. Henne, W. M.; Stenmark, H.; Emr, S. D., Molecular mechanisms of the membrane sculpting ESCRT pathway. *Cold Spring Harb. Perspect. Biol.* **2013,** *5* (9).

55. Carlton, J. G.; Agromayor, M.; Martin-Serrano, J., Differential requirements for Alix and ESCRT-III in cytokinesis and HIV-1 release. *Proc Natl Acad Sci U S A* **2008,** *105* (30), 10541-6.

56. Schmidt, O.; Teis, D., The ESCRT machinery. *Curr. Biol.* **2012,** *22* (4), R116-20.

57. Dowlatshahi, Dara P.; Sandrin, V.; Vivona, S.; Shaler, Thomas A.; Kaiser, Stephen E.; Melandri, F.; Sundquist, Wesley I.; Kopito, Ron R., ALIX Is a lys63-specific polyubiquitin binding protein that functions in retrovirus budding. *Dev. Cell* **2012,** *23* (6), 1247-1254.

58. Bissig, C.; Gruenberg, J., ALIX and the multivesicular endosome: ALIX in Wonderland. *Trends Cell Biol.* **2014,** *24* (1), 19-25.

59. Elias, R. D.; Ma, W.; Ghirlando, R.; Schwieters, C. D.; Reddy, V. S.; Deshmukh, L., Proline-rich domain of human ALIX contains multiple TSG101-UEV interaction sites and forms phosphorylation-mediated reversible amyloids. *Proc. Natl. Acad. Sci. U.S.A.* **2020,** *117* (39), 24274-24284.

60. Elias, R. D.; Ramaraju, B.; Deshmukh, L., Mechanistic roles of tyrosine phosphorylation in reversible amyloids, autoinhibition, and endosomal membrane association of ALIX. *J. Biol. Chem.* **2021,** *297* (5), 101328.

61. Dores, M. R.; Lin, H.; N, J. G.; Mendez, F.; Trejo, J., The α-arrestin ARRDC3 mediates ALIX ubiquitination and G protein-coupled receptor lysosomal sorting. *Mol. Biol. Cell* **2015,** *26* (25), 4660-73.

62. Sette, P.; Jadwin, J. A.; Dussupt, V.; Bello, N. F.; Bouamr, F., The ESCRT-associated protein ALIX recruits the ubiquitin ligase NEDD4-1 to facilitate HIV-1 release through the LYPXnL L domain motif. *J. Virol.* **2010,** *84* (16), 8181-92.

63. Zhai, Q.; Landesman, M. B.; Robinson, H.; Sundquist, W. I.; Hill, C. P., Identification and structural characterization of the ALIX-binding late domains of simian immunodeficiency virus SIVmac239 and SIVagmTan-1. *J. Virol.* **2011,** *85* (1), 632-7.

64. Swatek, K. N.; Komander, D., Ubiquitin modifications. *Cell Res.* **2016,** *26* (4), 399-422.

65. Kaiser, S. E.; Riley, B. E.; Shaler, T. A.; Trevino, R. S.; Becker, C. H.; Schulman, H.; Kopito, R. R., Protein standard absolute quantification (PSAQ) method for the measurement of cellular ubiquitin pools. *Nat. Methods* **2011,** *8* (8), 691-696.

66. Nakagawa, T.; Nakayama, K., Protein monoubiquitylation: targets and diverse functions. *Genes Cells* **2015,** *20* (7), 543-62.

67. Stefanis, L., α-Synuclein in Parkinson's disease. *Cold Spring Harb. Perspect. Med.* **2012,** *2* (2), a009399.

68. Conway, J. A.; Kinsman, G.; Kramer, E. R., The role of NEDD4 E3 ubiquitin–protein ligases in Parkinson's disease. *Genes* **2022,** *13* (3), 513.

69. Tofaris, G. K.; Razzaq, A.; Ghetti, B.; Lilley, K. S.; Spillantini, M. G., Ubiquitination of α-synuclein in Lewy bodies is a pathological event not associated with impairment of proteasome function. *J. Biol. Chem.* **2003,** *278* (45), 44405-11.

70. Odorizzi, G., The multiple personalities of ALIX. *J. Cell Sci.* **2006,** *119* (15), 3025-3032.

71. Laporte, M. H.; Chatellard, C.; Vauchez, V.; Hemming, F. J.; Deloulme, J.-C.; Vossier, F.; Blot, B.; Fraboulet, S.; Sadoul, R., ALIX is required during development for normal growth of the mouse brain. *Sci. Rep.* **2017,** *7* (1), 44767.

72. Korbei, B., Ubiquitination of the ubiquitin-binding machinery: how early ESCRT components are controlled. *Essays Biochem.* **2022,** *66* (2), 169-177.

73. Kim, T.; Chokkalla, A. K.; Vemuganti, R., Deletion of ubiquitin ligase NEDD4L exacerbates ischemic brain damage. *J. Cereb. Blood Flow Metab.* **2021,** *41* (5), 1058-1066.

74. Dores, M. R.; Lin, H.; Grimsey, N. J.; Mendez, F.; Trejo, J., The α-arrestin ARRDC3 mediates ALIX ubiquitination and G protein–coupled receptor lysosomal sorting. *Mol. Biol. Cell* **2015,** *26* (25), 4660-4673.

75. Hejjaoui, M.; Haj-Yahya, M.; Kumar, K. S. A.; Brik, A.; Lashuel, H. A., Towards elucidation of the role of ubiquitination in the pathogenesis of Parkinson's disease with semisynthetic ubiquitinated α-synuclein. *Angew. Chem., Int. Ed. Engl.* **2011,** *50* (2), 405-409.

76. Haj-Yahya, M.; Fauvet, B.; Herman-Bachinsky, Y.; Hejjaoui, M.; Bavikar, S. N.; Karthikeyan, S. V.; Ciechanover, A.; Lashuel, H. A.; Brik, A., Synthetic polyubiquitinated α-Synuclein reveals important insights into the roles of the ubiquitin chain in regulating its pathophysiology. *Proc. Natl. Acad. Sci. U.S.A.* **2013,** *110* (44), 17726-17731.

77. Meier, F.; Abeywardana, T.; Dhall, A.; Marotta, N. P.; Varkey, J.; Langen, R.; Chatterjee, C.; Pratt, M. R., Semisynthetic, site-specific ubiquitin modification of α-synuclein reveals differential effects on aggregation. *J. Am. Chem. Soc.* **2012,** *134* (12), 5468-5471.

78. Elias, R. D.; Zu, Y.; Su, Q.; Ghirlando, R.; Zhang, J.; Deshmukh, L., Gel-like condensates of human ALIX modulate the abscission checkpoint. **submitted**.

79. Schmidt, T. G. M.; Batz, L.; Bonet, L.; Carl, U.; Holzapfel, G.; Kiem, K.; Matulewicz, K.; Niermeier, D.; Schuchardt, I.; Stanar, K., Development of the Twin-Strep-tag and its application for purification of recombinant proteins from cell culture supernatants. *Protein Expr. Purif.* **2013,** *92* (1), 54-61.

80. Erlendsson, S.; Teilum, K., Binding revisited—avidity in cellular function and signaling. *Front. Mol. Biosci.* **2021,** *7*.

81. Li, Y.; Evers, J.; Luo, A.; Erber, L.; Postler, Z.; Chen, Y., A quantitative chemical proteomics approach for site-specific stoichiometry analysis of ubiquitination. *Angew. Chem., Int. Ed. Engl.* **2019,** *58* (2), 537-541.

82. Tofaris, G. K.; Kim, H. T.; Hourez, R.; Jung, J. W.; Kim, K. P.; Goldberg, A. L., Ubiquitin ligase Nedd4 promotes alpha-synuclein degradation by the endosomal-lysosomal pathway. *Proc. Natl. Acad. Sci. U.S.A.* **2011,** *108* (41), 17004-9.

83. Keren-Kaplan, T.; Attali, I.; Estrin, M.; Kuo, L. S.; Farkash, E.; Jerabek-Willemsen, M.; Blutraich, N.; Artzi, S.; Peri, A.; Freed, E. O.; Wolfson, H. J.; Prag, G., Structure-based in silico identification of ubiquitin-binding domains provides insights into the ALIX-V:ubiquitin complex and retrovirus budding. *EMBO J.* **2013,** *32* (4), 538-551.

84. Geiss-Friedlander, R.; Melchior, F., Concepts in sumoylation: a decade on. *Nat. Rev. Mol. Cell Biol.* **2007,** *8* (12), 947-956.

85. Ramaraju, B.; Nelson, S. L.; Zheng, W.; Ghirlando, R.; Deshmukh, L., Quantitative NMR study of insulin-degrading enzyme using amyloid-beta and HIV-1 p6 elucidates its chaperone activity. *Biochemistry* **2021,** *60* (33), 2519-2523.

86. Huth, J. R.; Bewley, C. A.; Jackson, B. M.; Hinnebusch, A. G.; Clore, G. M.; Gronenborn, A. M., Design of an expression system for detecting folded protein domains and mapping macromolecular interactions by NMR. *Protein Sci.* **1997,** *6* (11), 2359-64.

87. Cox, J.; Mann, M., MaxQuant enables high peptide identification rates, individualized p.p.b.-range mass accuracies and proteome-wide protein quantification. *Nat. Biotechnol.* **2008,** *26* (12), 1367-72.

88. Rückert, M.; Otting, G., Alignment of biological macromolecules in novel nonionic liquid crystalline media for NMR experiments. *J. Am. Chem. Soc.* **2000,** *122* (32), 7793-7797.

89. Delaglio, F.; Grzesiek, S.; Vuister, G. W.; Zhu, G.; Pfeifer, J.; Bax, A., NMRPipe: A multidimensional spectral processing system based on UNIX pipes. *J. Biomol. NMR* **1995,** *6* (3), 277-293.

90. Vranken, W. F.; Boucher, W.; Stevens, T. J.; Fogh, R. H.; Pajon, A.; Llinas, M.; Ulrich, E. L.; Markley, J. L.; Ionides, J.; Laue, E. D., The CCPN data model for NMR spectroscopy: Development of a software pipeline. *Proteins: Struct. Funct. Genet.* **2005,** *59* (4), 687-696.

91. Clore, G. M.; Gronenborn, A. M., Determining the structures of large proteins and protein complexes by NMR. *Trends Biotechnol.* **1998,** *16* (1), 22-34.

92. Fitzkee, N. C.; Bax, A., Facile measurement of ^{1}H-^{15}N residual dipolar couplings in larger perdeuterated proteins. *J. Biomol. NMR* **2010,** *48* (2), 65-70.

93. Schwieters, C. D.; Bermejo, G. A.; Clore, G. M., Xplor-NIH for molecular structure determination from NMR and other data sources. *Protein Sci.* **2018,** *27* (1), 26-40.

94. Gidi, Y.; Bayram, S.; Ablenas, C. J.; Blum, A. S.; Cosa, G., Efficient one-step PEG-silane passivation of glass surfaces for single-molecule fluorescence studies. *ACS Appl. Mater. Interfaces* **2018,** *10* (46), 39505-39511.

95. Paravastu, A. K.; Qahwash, I.; Leapman, R. D.; Meredith, S. C.; Tycko, R., Seeded growth of β-amyloid fibrils from Alzheimer's brain-derived fibrils produces a distinct fibril structure. *Proc. Natl. Acad. Sci. U.S.A.* **2009,** *106* (18), 7443-7448.

96. Deshmukh, L.; Ghirlando, R.; Clore, G. M., Conformation and dynamics of the Gag polyprotein of the human immunodeficiency virus 1 studied by NMR spectroscopy. *Proc. Natl. Acad. Sci. U.S.A.* **2015,** *112* (11), 3374-9.

97. Clore, G. M.; Garrett, D. S., R-factor, free R, and complete cross-validation for dipolar coupling refinement of NMR structures. *J. Am. Chem. Soc.* **1999,** *121* (39), 9008-9012.

98. Geoghegan, K. F.; Dixon, H. B.; Rosner, P. J.; Hoth, L. R.; Lanzetti, A. J.; Borzilleri, K. A.; Marr, E. S.; Pezzullo, L. H.; Martin, L. B.; LeMotte, P. K.; McColl, A. S.; Kamath, A. V.; Stroh, J. G., Spontaneous alpha-N-6-phosphogluconoylation of a "His tag" in Escherichia coli: the cause of extra mass of 258 or 178 Da in fusion proteins. *Anal. Biochem.* **1999,** *267* (1), 169-84.